J|A|C|S
ARTICLES
Published on Web 02/25/2003

# Mechanism and Energetics of Intramolecular Hydrogen Transfer in Amide and Peptide Radicals and Cation-Radicals

František Tureček* and Erik A. Syrstad

*Contribution from the Department of Chemistry, Bagley Hall, Box 351700, University of Washington, Seattle, Washington 98195-1700*

Received September 9, 2002; Revised Manuscript Received January 16, 2003; E-mail: turecek@chem.washington.edu

***Abstract:*** Intramolecular hydrogen transfer in five model amide and peptide radicals and cation-radicals was investigated by combined B3LYP-MP2 calculations. Hypervalent ammonium radicals produced by electron capture in protonated peptides undergo competitive elimination of ammonia, H-atom loss, and H-atom migration to neighboring amide carbonyls. The calculated transition state energies for H-atom migration are slightly but uniformly lower than those for H-atom loss. Transition state theory calculations with inclusion of quantum tunneling effects predict *k*(H migration)/*k*(H loss) branching ratios that increase with the ring size of the cyclic transition state for the migration. Intramolecular hydrogen-atom migration in amide and peptide radicals can be described by the proton-coupled electron transfer mechanism. The migrating hydrogen atom shows a negligible spin density and substantial positive charge that are typical of a proton migration. Electron transfer occurs through a $\pi$-orbital system and proceeds in the same (clockwise) or opposite (counterclockwise) direction as the proton motion, depending on the electronic properties of the chain connecting the ammonium group and the amide bond.

## Introduction

Hydrogen-atom transfer occurs in peptide and protein radicals as a result of radiation or oxidative damage and mainly involves the $C_\alpha-H$ bonds in glycine, S−H bond in cysteine, and O−H bond in tyrosine residues.[1] Hydrogen-atom transfer is also important for the functioning of some enzymes, for example, ribonucleotide reductase[2−4] and formate lyase dehydrogenase.[5,6] A different type of hydrogen-atom transfer has been considered to explain dissociations of multiply charged gas-phase peptide and protein ions following partial neutralization by capture of a thermal electron, termed electron capture dissociation (ECD).[7] According to one ECD mechanism, electron capture occurs at a protonated group in the multiply charged ion, which is typically the side-chain ammonium group of a lysine residue, the guanidinium group of an arginine residue, or an N-terminal ammonium group.[8] These protonated functionalities can be internally solvated by hydrogen bonding to other side-chain groups or to the amide oxygen atoms of the peptide backbone. Electron capture at the ammonium group produces a hypervalent 9-N-4 radical[9] which dissociates readily by expelling a hydrogen atom. The H atom is recaptured by an amide group to produce a transient amino ketyl radical that dissociates by cleavage of the $C(OH)NH-C_\alpha$ bond yielding complementary fragments containing the peptide N-terminus (termed *c*-series ions) and C-terminus (termed *z*-series ions).[10] Although this mechanism has been applied to explain ion dissociations,[11] there are several unresolved issues to be explained.

First, the energetics of electron capture by ammonium and guanidinium cations has not been elucidated for peptide ions or model systems. Second, hydrogen-atom transfer from the ammonium to the amide group can be visualized either as a dissociation−recapture involving two transition states or as a migration proceeding through a single transition state (Scheme 1). Experimental data are inconclusive in this respect, as reports using multiply charged $[\text{ubiquitin} + n\text{H}]^{n+}$ ($n = 8-12$) ions presented very different spectra that could be interpreted by either mechanism.[8,12] Third, prior to ECD reports, intramolecular hydrogen-atom transfer in hypervalent radicals was studied by experiment and theory with isomeric hexenylammonium[13] and hexenyldimethyloxonium radicals,[14] in which the hypervalent

(1) Hawkins, C. L.; Davies, M. J. *Biochim. Biophys. Acta* **2001**, *1504*, 196−219.
(2) Sun, X.; Harder, J.; Krook, M.; Jornvall, H.; Sjoberg, B. M.; Reichard, P. *Proc. Natl. Acad. Sci. U.S.A.* **1993**, *90*, 577−581.
(3) Mulliez, E.; Fontecave, M.; Gaillard, J.; Reichard, P. *J. Biol. Chem.* **1993**, *268*, 2296−2299.
(4) Sun, X.; Eliasson, R.; Pontis, E.; Andersson, J.; Buist, G.; Sjoberg, B. M.; Reichard, P. *J. Biol. Chem.* **1995**, *270*, 2443−2446. For a review, see: Jordan, A.; Reichard, P. *Annu. Rev. Biochem.* **1998**, *67*, 71−98.
(5) Knappe, J.; Neugebauer, F. A.; Blaschkowski, H. P.; Ganzler, M. *Proc. Natl. Acad. Sci. U.S.A.* **1984**, *81*, 1332−1335.
(6) Parast, C. V.; Wong, K. K.; Lewisch, S. A.; Kozarich, J. W.; Peisach, J.; Magliozzo, R. S. *Biochemistry* **1995**, *34*, 2393−2399.
(7) (a) Zubarev, R. A.; Kelleher, N. L.; McLafferty, F. W. *J. Am. Chem. Soc.* **1998**, *120*, 3265−3266. (b) Kruger, N. A.; Zubarev, R. A.; Carpenter, B. K.; Kelleher, N. L.; Horn, D. M.; McLafferty, F. W. *Int. J. Mass Spectrom.* **1999**, *182*/*183*, 1−5.
(8) Zubarev, R. A.; Kruger, N. A.; Fridriksson, E. K.; Lewis, M. A.; Horn, D. M.; Carpenter, B. K.; McLafferty, F. W. *J. Am. Chem. Soc.* **1999**, *121*, 2857−2862.
(9) Perkins, C. W.; Martin, J. C.; Arduengo, A. J.; Lau, W.; Alegria, A.; Kochi, J. K. *J. Am. Chem. Soc.* **1980**, *102*, 7753.
(10) For peptide fragment nomenclature, see: (a) Roepstorff, P.; Fohlman, J. *Biomed. Mass Spectrom.* **1984**, *11*, 601. (b) Biemann, K. *Biomed. Environ. Mass Spectrom.* **1988**, *16*, 99.
(11) Polfer, N. C.; Haselmann, K. F.; Zubarev, R. S. A.; Langridge-Smith, P. R. R. *Rapid Commun. Mass Spectrom.* **2002**, *16*, 936−943.
(12) Breuker, K.; Oh, H. B.; Cerda, B. A.; Horn, D. M.; McLafferty, F. W. *Eur. Mass Spectrom.* **2002**, *8*, 177−180.

10.1021/ja021162t CCC: $25.00 

***Scheme 1***

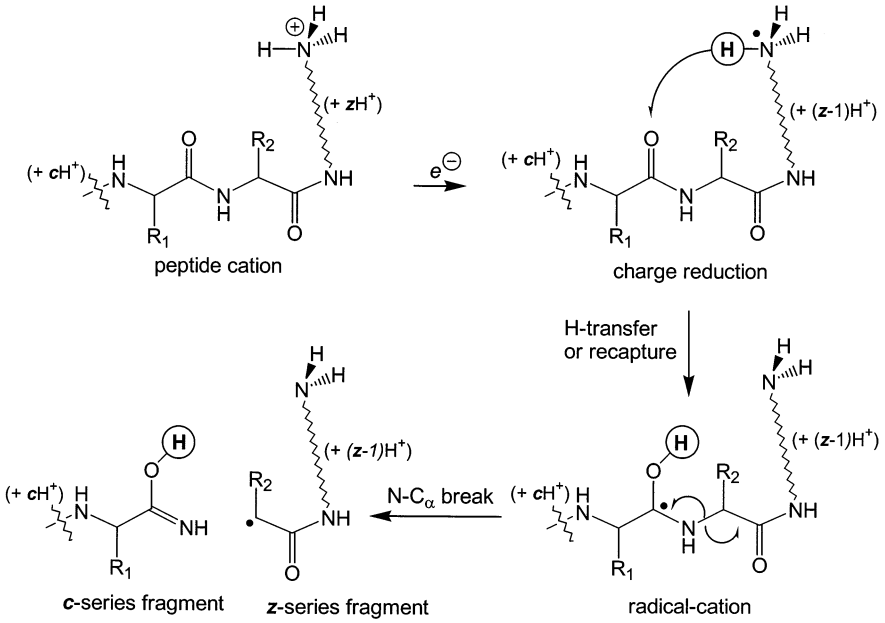


***Scheme 2***

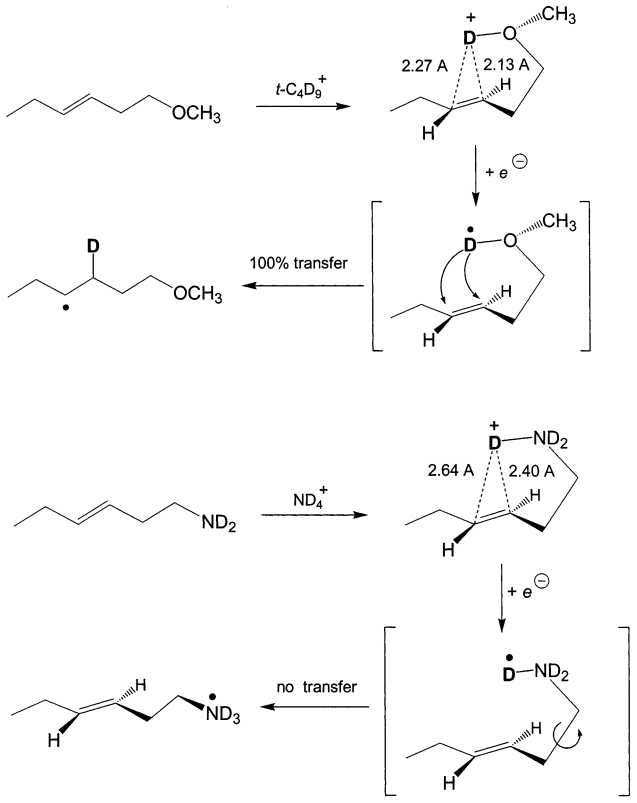


ammonium or oxonium groups served as hydrogen-atom donors and the double bond served as an acceptor (Scheme 2). The transient radicals were generated by femtosecond collisional electron transfer to the corresponding cations in which one proton of the incipient donor group and the double bond were held in proximity by intramolecular hydrogen bonding. Interestingly, while hydrogen-atom transfer was efficient in the oxonium radicals, it did not occur in the ammonium radicals. This was explained by differences in the potential energy surfaces. Hypervalent oxonium radicals are unbound and release the hydrogen atom exothermically and without a barrier, so that hydrogen transfer can proceed by the dissociation−recapture mechanism. The kinetic energy of the released hydrogen atom was estimated to be sufficient to overcome a small potential energy barrier for addition to a C═C double bond.[14] In contrast, hypervalent ammonium radicals are weakly bound along the N−H coordinate. Electron capture disrupts the hydrogen bonding to the C═C bond and results in an exothermic rotation of the $NH_3$ group away from the double bond, so that hydrogen transfer is hampered. Finally, hydrogen-atom additions to amide bonds have substantial activation energies, as studied for simple models, formamide[15] and *N*-methyl acetamide,[16] that can affect the hydrogen transfer kinetics and mechanism.

Another ECD mechanism has been proposed recently[17] that presumes electron capture in a Rydberg orbital of the multiply charged peptide ion followed by direct N−C bond cleavage in an excited electronic state. This mechanism had been put forth prior to ECD to explain dissociations of aromatic ammonium ions following femtosecond electron transfer.[18] However, reaction mechanisms are difficult to study with protein or even oligopeptide ions, because the accurate structure of the reactant is often unknown due to the presence of multiple ion tautomers differing in proton positions, and multiple conformers of each structure. Reaction energetics is usually unavailable, and accurate structures of the dissociation products are also unknown. However, ECD can provide very useful information on the amino acid sequence, and so gaining an understanding of the dissociation mechanisms is of interest and warrants model studies with simpler molecular systems.

(13) Shaffer, S. A.; Sadílek, M.; Tureček, F.; Hop, C. E. C. A. *Int. J. Mass Spectrom. Ion Processes* **1997**, *160*, 137−155.
(14) Shaffer, S. A.; Wolken, J. K.; Tureček, F *J. Am. Soc. Mass Spectrom.* **1997**, *8*, 1111−1123.
(15) Syrstad, E. A.; Turecek, F. *J. Phys. Chem. A* **2001**, *105*, 11144−11155.
(16) Syrstad, E. A.; Stephens, D. D.; Turecek, F. *J. Phys. Chem. A* **2003**, *107*, 115−126.
(17) Hudgins, R. R.; Hakansson, K.; Quinn, J. P.; Hendrickson, C. L.; Marshall, A. G. *Proceedings of the 50th Annual Conference on Mass Spectrometry and Allied Topics*; Orlando, FL, June 2002.
(18) Shaffer, S. A.; Sadílek, M.; Tureček, F. *J. Org. Chem.* **1996**, *61*, 5234−5245.

In the context of the recent discussion of ECD mechanisms,[7,8,19−21] we now investigate the energetics and mechanisms of hydrogen-atom transfer in model amide and peptide systems. In the present work, we use ab initio and density functional theory calculations to study model amide systems of increasing complexity. The systems of models 1−3 deal with hydrogen-atom transfer from the ammonium N-terminus in $\beta$-alanine amide and *N*-methylamide radicals. Model 4 concerns hydrogen-atom transfer from the C-terminus in *N*-acetyl ethylenediamine radicals. Finally, model 5 deals with hydrogen-atom transfer from the N-terminus in ammonium radicals derived from glycylglycinamide, Gly−Gly−$NH_2$. Of interest are the potential energy barriers for H-atom dissociation, recapture, and transfer, and the electronic properties of the reactants and transition states. In particular, we wish to show that H-atom transfer in peptide ammonium radicals follows the proton-coupled electron transfer (PCET) mechanism introduced by Siegbahn and co-workers[22,23] and applied to several organometallic[24] and organic reactions.[25]

## Calculations

Standard ab initio and density functional theory calculations were performed with the Gaussian 98 suite of programs.[26] Optimized geometries were obtained with density functional theory calculations using Becke's hybrid functional, B3LYP,[27] and the 6-31+G(d,p) or 6-31++G(d,p) basis sets. These gave very similar structures that could be used interchangeably for single-point energy calculations. Harmonic frequencies were calculated to characterize stationary states as local minima (all real frequencies) and first-order saddle points (one imaginary frequency). Complete optimized geometries are available as Supporting Information; harmonic frequencies can be obtained from the corresponding author upon request. Single-point energies were obtained with B3LYP and Moller−Plesset perturbational calculations[28] truncated at second order, MP2, with frozen core and valence electron only excitations. The basis sets in the single-point calculations were 6-311++G(2df,p) for the systems of models 1−4 and 6-311++G(2d,p) for model 5 systems. Spin contamination in calculations with spin unrestricted wave functions was negligible to moderate, as judged from the $\langle S^2 \rangle$ operator expectation values that were 0.75−0.76 for UB3LYP calculations of local minima and transition states, 0.75−0.77 for UMP2 calculations of local minima, and 0.76−0.96 for UMP2 calculations of transition states. Spin projection[29] (PMP2) reduced the $\langle S^2 \rangle$ values to 0.75−0.77 and resulted in total energy corrections of <5 mhartree (13 kJ mol$^{-1}$). The single-point energies from the B3LYP and spin-projected MP2 calculations were averaged and used to calculate B3-PMP2 relative energies that were corrected for zero-point vibrational energies and are discussed throughout. This empirical procedure[30,31] has been shown to result in efficient cancellation of small errors inherent to B3LYP and MP2 formalisms and to provide relative and activation energies that in accuracy compare favorably with or even supersede those from high level composite Gaussian 2 or Gaussian 2(MP2) calculations, as reported for several systems.[32] The errors inherent to the MP2 and B3LYP schemes have been analyzed by Rassolov, Ratner, and Pople and found to originate in part from underestimation and overestimation, respectively, of correlation energy.[33] For selected reactions, we also performed single-point calculations with quadratic configuration interaction including single, double, and perturbational triple excitations,[34] QCISD(T)/6-31++G-(d,p). These energies were extended to the larger basis set using a linear energy relationship, $E\{\text{QCISD(T)/6-311++G(2df,p)}\} \approx E\{\text{QCISD(T)/6-31++G(d,p)}\} + E\{\text{MP2/6-311++G(2df,p)}\} - E\{\text{MP2/6-31++G(d,p)}\}$. Radical excited-state energies were calculated for vertical excitations from optimized radical or cation geometries using the time-dependent density functional theory[35] with the B3LYP functional and 6-311++G(2d,p) basis set. Transition state theory (TST) calculations used the standard formula.[36] Rotational partition functions were obtained from the Gaussian 98 output files; vibrational partition functions were calculated from the B3LYP/6-31++G(d,p) harmonic frequencies.

## Results and Discussion

**Models 1−3 Ion and Radical Structures.** The $\beta$-alanine amide and *N*-methylamide ammonium cations and radicals of the systems of models 1−3 show very similar structure features that are illustrated here with the simplest model 1 structures. Cation **1a**$^+$ has an elongated equatorial N−H bond (1.081 Å), and the proton has a short hydrogen bond (1.574 Å) to the amide oxygen atom (Scheme 3). The strength of the N−H···O hydrogen bond in **1a**$^+$ can be estimated from the enthalpy difference between **1a**$^+$ and the non-H-bonded anti-isomer **1c**$^+$, $\Delta H_{\text{rxn,298}}$ (**1a**$^+ \rightarrow$ **1c**$^+$) = 59 kJ mol$^{-1}$, favoring **1a**$^+$. Ion **1c**$^+$ is


(19) Cooper, H. J.; Hudgins, R. R.; Hakansson, K.; Marshall, A. G. *J. Am. Soc. Mass Spectrom.* **2002**, *13*, 241−249.
(20) Tureček, F. *Proceedings of the 50th Annual Conference on Mass Spectrometry and Allied Topics*; Orlando, FL, June 2002.
(21) Konishi, H.; Yokotake, Y.; Ishibashi, T. *J. Mass Spectrom Soc. Jpn.* **2002**, *50*, 229−232.
(22) Siegbahn, P. E. M.; Blomberg, M. R. A.; Crabtree, R. H. *Theor. Chim. Acc.* **1997**, *97*, 289−300.
(23) Siegbahn, P. E. M.; Eriksson, L.; Himo, F.; Pavlov, M. *J. Phys. Chem. B* **1998**, *102*, 10622−10629.
(24) Cujier, R. I.; Nocera, D. G. *Annu. Rev. Phys. Chem.* **1998**, *49*, 337−369.
(25) Mayer, J. M.; Hrovat, D. A.; Thomas, J. L.; Borden, W. T. *J. Am. Chem. Soc.* **2002**, *124*, 11142−11147.
(26) Frisch, M. J.; Trucks, G. W.; Schlegel, H. B.; Scuseria, G. E.; Robb, M. A.; Cheeseman, J. R.; Zakrzewski, V. G.; Montgomery, J. A., Jr.; Stratmann, R. E.; Burant, J. C.; Dapprich, S.; Millam, J. M.; Daniels, A. D.; Kudin, K. N.; Strain, M. C.; Farkas, O.; Tomasi, J.; Barone, V.; Cossi, M.; Cammi, R.; Mennucci, B.; Pomelli, C.; Adamo, C.; Clifford, S.; Ochterski, J.; Petersson, G. A.; Ayala, P. Y.; Cui, Q.; Morokuma, K.; Malick, D. K.; Rabuck, A. D.; Raghavachari, K.; Foresman, J. B.; Cioslowski, J.; Ortiz, J. V.; Stefanov, B. B.; Liu, G.; Liashenko, A.; Piskorz, P.; Komaromi, I.; Gomperts, R.; Martin, R. L.; Fox, D. J.; Keith, T.; Al-Laham, M. A.; Peng, C. Y.; Nanayakkara, A.; Gonzalez, C.; Challacombe, M.; Gill, P. M. W.; Johnson, B. G.; Chen, W.; Wong, M. W.; Andres, J. L.; Head-Gordon, M.; Replogle, E. S.; Pople, J. A. *Gaussian 98*, revision A.6; Gaussian, Inc.: Pittsburgh, PA, 1998.
(27) (a) Becke, A. D. *J. Chem. Phys.* **1993**, *98*, 1372, 5648. (b) Stephens, P. J.; Devlin, F. J.; Chabalowski, C. F.; Frisch, M. J. *J. Phys. Chem.* **1994**, *98*, 11623.
(28) Møller, C.; Plesset, M. S. *Phys. Rev.* **1934**, *46*, 618−622.
(29) Schlegel, H. B. *J. Chem. Phys.* **1986**, *84*, 4530−4534.
(30) Tureček, F. *J. Phys. Chem. A* **1998**, *102*, 4703−4713.
(31) Rablen, P. R. *J. Am. Chem. Soc.* **2000**, *122*, 357−368.
(32) (a) Wolken, J. K.; Tureček, F. *J. Am. Chem. Soc.* **1999**, *121*, 6010−6018. (b) Wolken, J. K.; Tureček, F. *J. Phys. Chem. A* **1999**, *103*, 6268−6281. (c) Tureček, F.; Polášek, M.; Frank, A. J.; Sadílek, M. *J. Am. Chem. Soc.* **2000**, *122*, 2361−2370. (d) Polášek, M.; Tureček, F. *J. Am. Chem. Soc.* **2000**, *122*, 9511−9524. (e) Wolken, J. K.; Tureček, F. *J. Am. Soc. Mass Spectrom.* **2000**, *11*, 1065−1071. (f) Tureček, F. *J. Mass Spectrom.* **2000**, *35*, 1351−1359. (g) Wolken, J. K.; Syrstad, E. A.; Vivekananda, S.; Tureček, F. *J. Am. Chem. Soc.* **2001**, *123*, 5804−5805. (h) Vivekananda, S.; Tureček, F.; Polášek, M. *J. Mass Spectrom.* **2002**, *37*, 829−839. (i) Tureček, F.; Vivekananda, S.; Sadilek, M.; Polášek, M. *J. Am. Chem. Soc.* **2002**, *124*, 13282−13289.
(33) Rassolov, V. A.; Ratner, M. A.; Pople, J. A. *J. Chem. Phys.* **2000**, *112*, 4014−4019.
(34) Pople, J. A.; Head-Gordon, M.; Raghavachari, K. *J. Chem. Phys.* **1987**, *87*, 5968−5975.
(35) Stratmann, R. E.; Scuseria, G. E.; Frisch, M. J. *J. Chem. Phys.* **1998**, *109*, 8218−8224.
(36) Levine, I. N. *Physical Chemistry*, 3rd ed.; McGraw-Hill: New York, 1988; p 846.

***Scheme 3***

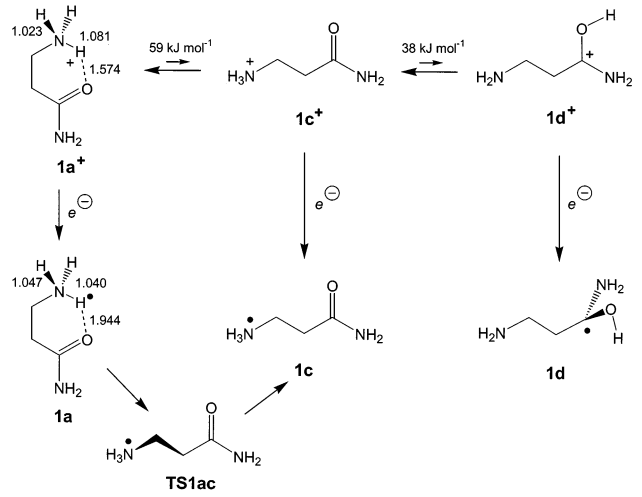


***Scheme 4***

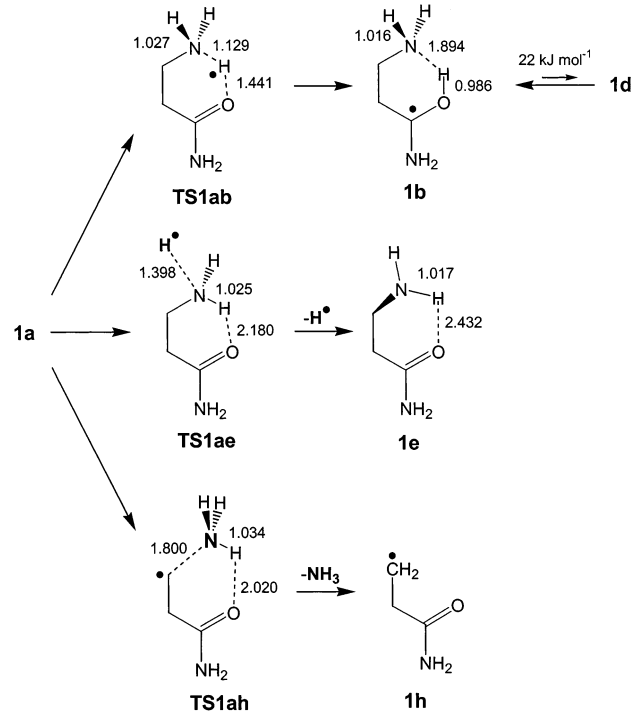


in turn 38 kJ mol$^{-1}$ more stable than the O-protonated tautomer **1d**$^+$ (Scheme 3). Electron capture in **1a**$^+$ results in substantial bond length changes in the resulting radical **1a**. In particular, the equatorial N−H bond is shorter in **1a** (1.040 Å), while the O···H distance increases to 1.944 Å (Scheme 3). This is evidence of the weakening of the hydrogen bond in **1a**. Additional evidence stems from the enthalpy difference between **1a** and the open-chain radical **1c**, $\Delta H_{rxn,298}$ (**1a** → **1c**) = 1 kJ mol$^{-1}$, which only slightly favors **1a**.

Hydrogen transfer from the hypervalent ammonium group onto the amide carbonyl proceeds through a six-membered cyclic transition state (**TS1ab**). **TS1ab** is an early transition state with a slightly elongated N−H bond (1.129 Å), and a long newly forming O−H bond (1.441 Å, Scheme 4). The product **1b** is a ketyl radical in which the hydroxyl proton is hydrogen bonded to the amine nitrogen at a 1.894 Å N···H distance. The strength of the hydrogen bond in **1b** can be estimated from the energy difference between it and the open-chain ketyl radical **1d**,

***Table 1.*** Model 1 Relative Energies

| | relative energy[a] | | | | |
|---|---|---|---|---|---|
| | 6-31++G(d,p) | 6-311++G(2df,p) | | | |
| species/reaction | B3LYP | B3LYP | PMP2 | B3-PMP2 | QCISD(T)[b] |
| **1a** → **1b** | −64 | −65 | −68 | −66 | −73 |
| **1a** → **TS1ab** | 1 | 0.5 | 29 | 15 | 45 |
| **1a** → **1c** | 3 | 2 | −1 | 1 | |
| **1a** → **TS1ac** | 13 | 13 | 12 | 12 | |
| **1a** → **TS1aa** | 14 | 13 | 15 | 14 | |
| **1a** → **1g** | −3 | −3 | 26 | 12 | |
| **1a** → **1e** + H• | −3 | −11 | −43 | −27 | −32 |
| **1a** → **TS1ae** | 13 | 11 | 8 | 10 | 11 |
| **1a** → $NH_3$ + **1h** | −105 | −115 | −103 | −109 | |
| **1a** → **TS1ah** | 28 | 27 | 56 | 41 | |
| **1b** → **1d** | 22 | 20 | 21 | 21 | 20 |
| **1d** → **TS1fd** | 71 | 69 | 68 | 68 | |
| **1d** → **1f** + H• | 45 | 41 | 13 | 27 | |
| **1c** → **TS1cf** | 16 | 14 | 16 | 15 | |
| **1f** + H• → **TS1fd** | 27 | 28 | 56 | 42 | |
| **1f** + H• → **TS1cf** | 16 | 22 | 51 | 36 | 43 |
| **1e** + H• → **1g** | 1 | 9 | 69 | 39 | |
| **1e** + H• → **TS1eg** | 44 | 46 | 66 | 56 | |
| **1j**$^{+\bullet}$ → **1k**$^{+\bullet}$ | 35 | 34 | 34 | 34 | 33 |
| **1j**$^{+\bullet}$ → **1a**$^+$ + H• | 44 | 39 | 10 | 24 | 27 |
| **1j**$^{+\bullet}$ → **TS1ja** | 84 | 82 | 81 | 81 | 95 |
| **1a**$^+$ + H• → **TS1ja** | 40 | 43 | 71 | 57 | 68 |

[a] In units of kJ mol$^{-1}$ at 0 K including B3LYP/6-31++G(d,p) zero-point energy corrections. [b] Effective energies $E$[QCISD(T)/6-311++G(2df,p)] ≈ $E$[QCISD(T)/6-31++G(d,p)] + $E$[PMP2/6-311++G(2df,p)] − $E$[PMP2/6-31++G(d,p)].

***Scheme 5***

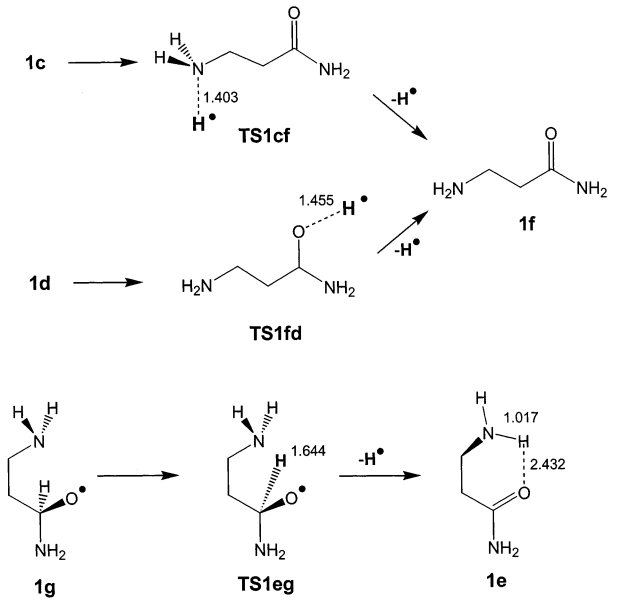


$\Delta H_{rxn,298}$ (**1b** → **1d**) = 22 kJ mol$^{-1}$, in favor of **1b** (Table 1). By comparison, with $\beta$-alanine amide isomers, hydrogen bonding between the amine and carbonyl group stabilizes **1e** by 7.5 kJ mol$^{-1}$ relative to the open-chain isomer **1f** at 298 K (Scheme 5). Model 2 and model 3 molecules, cations, and radicals consist of cis- and trans-amide isomers, respectively, that differ in the orientation of the *N*-methyl group (Schemes 6 and 8). The N−H and O−H bond lengths in model 2 and model 3 species are similar to those in $\beta$-alanine amide species and to each other as well. In general, the trans-amide isomers are more stable than the cis-isomers. However, the trans → cis energy difference depends on the species in question. Trans-cations (**2a**$^+$), radicals (**2a**), and neutral amides (**2c**) are 10.1, 9.2, and 9.3 kJ mol$^{-1}$

***Scheme 6***

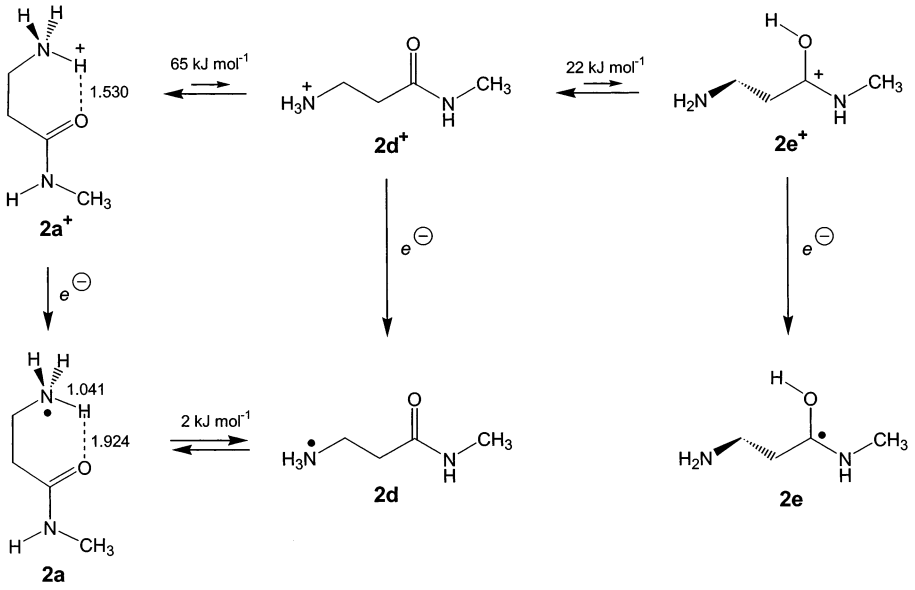


***Scheme 7***

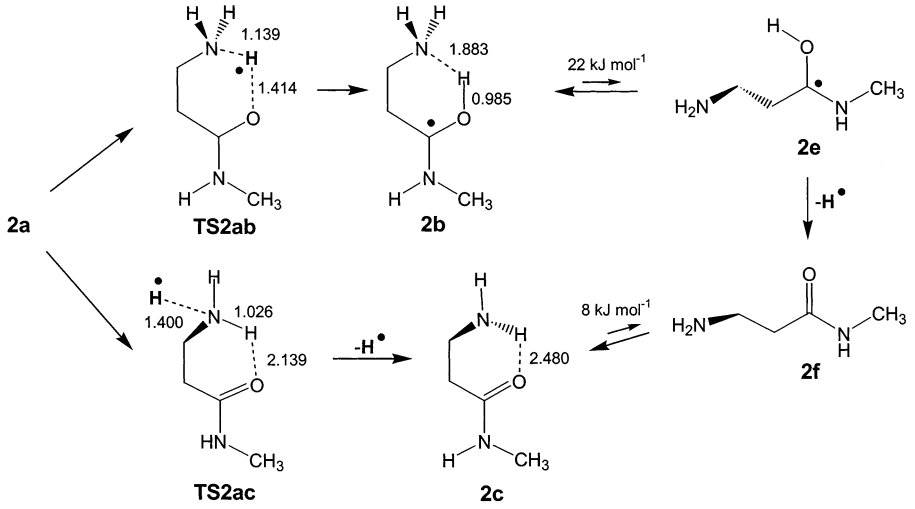


more stable than the respective cis-isomers, **3a**$^+$, **3a**, and **3c** (Table 2, 0 K values). In contrast, the trans-ketyl radical **2b** is calculated to be only 0.4 kJ mol$^{-1}$ more stable than **3b**, and so these cis−trans radical isomers can be considered isoenergetic at the present level of theory. Intramolecular hydrogen bonding is strongest between the ammonium and carbonyl group in **2a**$^+$ where unfolding the chain requires 65 kJ mol$^{-1}$ to form **2d**$^+$ (Scheme 6). Hydrogen bonding is much weakened in ammonium radicals **2a** and **3a** where unfolding to **2d** and **3d**, respectively, requires only 2 kJ mol$^{-1}$. Unfolding in neutral amides **2c** and **3c** is 8 and 12 kJ mol$^{-1}$ endothermic to form **2f** and **3f**, respectively. Hydrogen bonding slightly increases in ketyl radicals **2b** (Scheme 7) and **3b** (Scheme 9) where unfolding is 22 kJ mol$^{-1}$ endothermic to form **2e** and **3e**, respectively.

**Reaction Energetics of Models 1−3.** The radicals of the systems of models 1−3 can undergo several unimolecular reactions. The pertinent transition state (TS) and reaction energies are summarized in Tables 1 and 2. In the text, we discuss the B3-PMP2 energies and point out discrepancies between results from different levels of theory wherever significant. The weak hydrogen bond in **1a** is indicated by the low TS energies for rotation of the hypervalent $NH_3$ group (**TS1aa**, $E_{TS1aa} = 14$ kJ mol$^{-1}$, structure not shown) and chain unfolding to **1c** (**TS1ac**, $E_{TS1ac} = 12$ kJ mol$^{-1}$). Dissociation of one of the N−H bonds in **1c** requires 15 kJ mol$^{-1}$ in **TS1cf** and is overall 20 kJ mol$^{-1}$ exothermic to form the $\beta$-alanine amide conformer **1f**. Direct cleavage of one of the out-of-plane N−H bonds in **1a** is even more facile, requiring 10 kJ mol$^{-1}$ in **TS1ae** and forming the more stable hydrogen-bonded $\beta$-alanine amide conformer **1e**. These energies indicate very facile bond dissociation in hypervalent ammonium radicals of the model 1 system, in keeping with previous studies of simple aliphatic ammonium radicals.[37]

Hydrogen migration, **1a** → **1b**, proceeds through **TS1ab** which is 15 kJ mol$^{-1}$ above **1a**. The isomerization is 66 kJ mol$^{-1}$ exothermic, but the internal energy gained by **1b** is insufficient

(37) (a) Gellene, G. I.; Porter, R. F. *Acc. Chem. Res.* **1983**, *16*, 200−207. (b) Williams, B. W.; Porter, R. F. *J. Chem. Phys.* **1980**, *73*, 5598−5604. (c) Gellene, G. I.; Cleary, D. A.; Porter, R. F. *J. Chem. Phys.* **1982**, *77*, 3471−3477. (d) Boldyrev, A. I.; Simons, J. *J. Chem. Phys.* **1992**, *97*, 6621−6627. (e) Nguyen, V. Q.; Sadílek, M.; Frank, A. J.; Ferrier, J. G.; Tureček, F. *J. Phys. Chem. A* **1997**, *101*, 3789−3799. (f) Shaffer, S. A.; Tureček, F. *J. Am. Chem. Soc.* **1994**, *116*, 8647−8653. (g) Frøsig, L.; Tureček, F. *J. Am. Soc. Mass Spectrom.* **1998**, *9*, 242−254. (h) Sadílek, M.; Tureček, F. *J. Phys. Chem.* **1996**, *100*, 9610−9614.

***Scheme 8***

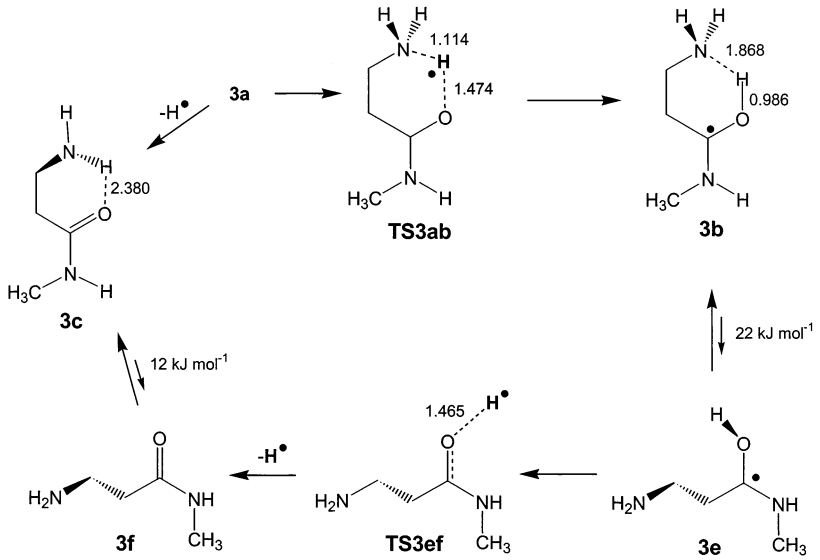


***Table 2.*** Energies of Models 2 and 3

| | relative energy[a] | | | |
|---|---|---|---|---|
| | 6-31++G(d,p) | 6-311++G(2df,p) | | |
| species/reaction | B3LYP | B3LYP | PMP2 | B3-PMP2 |
| **2a**$^+$ → **3a**$^+$ | 10 | 10 | 10 | 10 |
| **2a** → **3a** | 10 | 10 | 8 | 9 |
| **2b** → **3b** | −0.2 | 0.1 | 0.6 | 0.4 |
| **2c** → **3c** | 9 | 9 | 9 | 9 |
| **2a** → **2b** | −58 | −59 | −61 | −60 |
| **2a** → **TS2ab** | 3 | 4 | 32 | 18 |
| **2a** → **2d** | 4 | 3 | 1 | 2 |
| **2a** → **2c** + H• | −2 | −9 | −41 | −25 |
| **2a** → **TS2ac** | 13 | 12 | 10 | 11 |
| **2b** → **2e** | 23 | 21 | 23 | 22 |
| **2e** → **2f** + H• | 39 | 35 | 7 | 21 |
| **3a** → **3b** | −69 | −69 | −69 | −69 |
| **3a** → **TS3ab** | 0.7 | 0.7 | 25 | 13 |
| **3a** → **3c** + H• | −3 | −10 | −40 | −25 |
| **3e** → **3f** + H• | 51 | 47 | 19 | 33 |
| **3e** → **TS3ef** | 74 | 71 | 70 | 71 |

[a] In units of kJ mol$^{-1}$ at 0 K.

for cleavage of the ketyl O−H bond. This can proceed by endoergic chain unfolding, **1b** → **1d** (Scheme 4), followed by O−H bond dissociation through **TS1fd** (Scheme 5). Greater activation energies are calculated for the loss of $NH_3$ from **1a** (**TS1ah**, $E_{TS1ah}$ = 41 kJ mol$^{-1}$) and recapture of an H atom by the $\beta$-alanine amide carbonyl in **1f** (**TS1fd**, $E_{TS1fd}$ = 42 kJ mol$^{-1}$). Hydrogen-atom addition to the C atom of the amide bond of **1e** is 39 kJ mol$^{-1}$ endothermic to give the oxyradical **1g**, and it proceeds over a 56 kJ mol$^{-1}$ activation barrier in **TS1eg**.

The effect of an adjacent charge on the radical structure, H-atom capture, and loss was studied with cation-radical **1j**$^{+\bullet}$ which corresponds to O-protonated **1a** (Scheme 10). The hydrogen bonding between the ammonium and OH groups in **1j**$^{+\bullet}$ is weaker than in **1a**$^+$, as unfolding to the open-chain isomer **1k**$^{+\bullet}$ requires 34 kJ mol$^{-1}$ at 0 K (Table 1). Dissociation of the O−H bond in **1j**$^{+\bullet}$ is 24 kJ mol$^{-1}$ endothermic to produce **1a**$^+$, which is comparable to the analogous dissociation of **1d**. The exothermic recapture of the H atom by **1a**$^+$ requires 57 kJ mol$^{-1}$ in **TS1ja** (Table 1), indicating that amine group protonation and ammonium hydrogen bonding to the carbonyl in **1a**$^+$ disfavor H-atom addition.

The corrections by the B3-PMP2 scheme result in relative energies that are consistent with those from effective QCISD(T) calculations for the reactions **1a** → **1e** + H, **1f** + H → **TS1cf**, and **1j**$^{+\bullet}$ → **1a**$^+$ + H (Table 1). A notable exception is the energy for **TS1ab**, which shows a divergent trend in that the $E_{TS}$ increases from PMP2 to QCISD(T). This discrepancy is probably due to the proximity of closely spaced excited electronic states in **TS1ab**, as discussed in the pertinent section below.

The energetics in the model 2 and model 3 systems (Table 2) are quite similar to each other and to that of the model 1 system (Table 1). N−H bond dissociations in the hypervalent ammonium radicals are exothermic and require small activation energies, for example, $\Delta H_{rxn,0}$ = −25 kJ mol$^{-1}$ and $E_{TS}$ = 11 kJ mol$^{-1}$ for **2a** → **TS2ac** → **2c** + H. The activation energies for the N−H→O migration are 18 and 13 kJ mol$^{-1}$ for **2a** and **3a**, respectively, which are comparable to the barrier in **1a** (Table 1) and also show similar discrepancies between the B3LYP and PMP2 values. The activation energy for H-atom capture by the carbonyl oxygen in **3f** is 38 kJ mol$^{-1}$ in **TS3fe** which is comparable to the analogous barrier for H addition in **1f**. Hence, the calculated activation energies in the systems of models 1−3 indicate that the concerted H-atom transfer is energetically slightly more favorable than the two-step dissociation−recapture reaction.

**Model 4 Structures and Energetics.** Model 4 differs from models 1−3 in that hydrogen bonding and H-atom transfer occur in seven-membered cyclic structures or transition states where the proton or H atom approaches the carbonyl group from the "C-terminus" of the amide bond. The ammonium cation **4a**$^+$ shows a strong intramolecular hydrogen bond between one of the ammonium protons and the carbonyl oxygen, as evidenced by the 1.472 Å O···H distance. The hydrogen bonding is weakened in radical **4a**, which shows a 1.767 Å O···H distance (Scheme 11). Intramolecular hydrogen transfer in **4a** proceeds through an early TS (**TS4ab**), in which the N−H and O−H bond lengths, 1.142 and 1.396 Å, respectively, resemble those in ion **4a**$^+$ (Scheme 11). The resulting ketyl radical **4b** shows an O−H···N hydrogen bond (1.790 Å). An OH bond rotamer (**4c**) that has a weak O···H−N hydrogen bond (2.29 Å) is 19 kJ mol$^{-1}$ less stable than **4b**.

***Scheme 9***

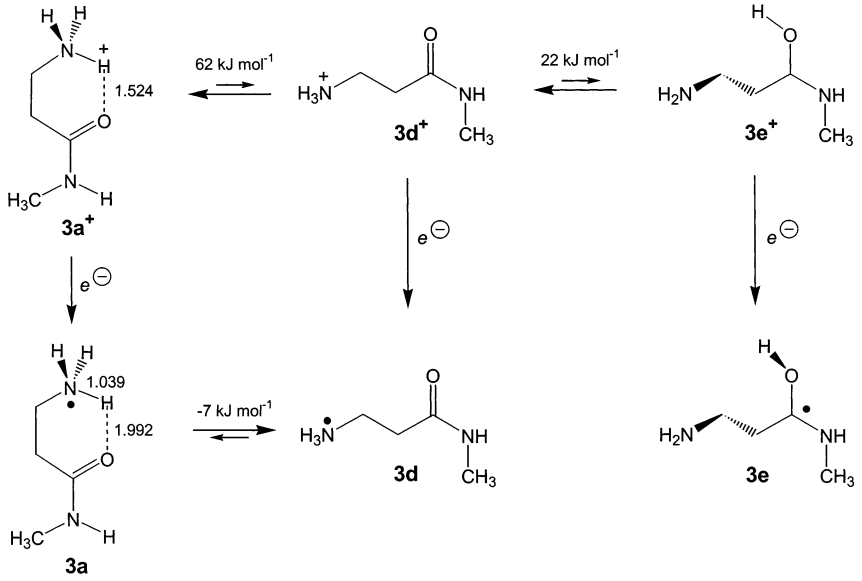


***Scheme 10***

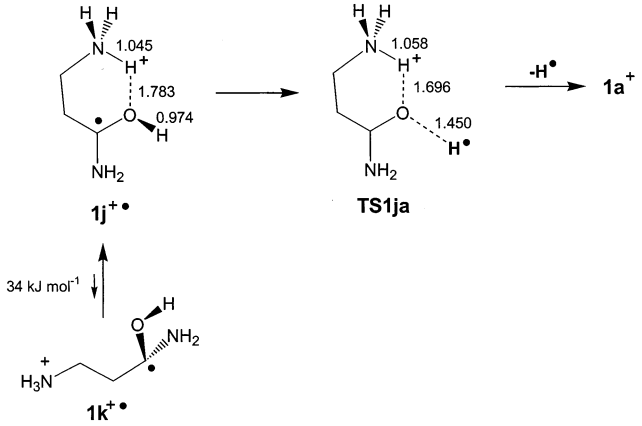


***Table 3.*** Model 4 Energies

| | relative energy[a] | | | | |
|---|---|---|---|---|---|
| | 6-31++G(d,p) | 6-311++G(2df,p) | | | |
| species/reaction | B3LYP | B3LYP | PMP2 | B3-PMP2 | QCISD(T)[b] |
| **4a** → **4d** + H• | −3 | −10 | −43 | −27 | −31 |
| **4a** → **TS4ad** | 14 | 12 | 7 | 10 | 11 |
| **4a** → **4b** | −62 | −63 | −67 | −65 | −73 |
| **4a** → **TS4ab** | −1 | 0.4 | 33 | 17 | 78 |
| **4b** → **4d** + H• | 59 | 53 | 24 | 38 | 41 |
| **4b** → **4c** | 21 | 19 | 20 | 19 | |
| **4b** → **TS4bc** | 24 | 21 | 23 | 22 | |
| **4c** → **TS4cd** | 70 | 68 | 71 | 70 | |
| **4e**+• → **4a**+ + H• | 36 | 31 | 4 | 17 | 21 |
| **4e**+• → **TS4ea** | 86 | 84 | 86 | 85 | |

[a] In units of kJ mol$^{-1}$ at 0 K. [b] Effective QCISD(T)/6-311++G(2df,p) energies.

The dissociation and isomerization energies pertinent to model 4 radicals are given in Table 3. Cleavage of an N−H bond in the hypervalent ammonium group in **4a** has a low energy barrier, **TS4ad**, $E_{TS4ad}$ = 10 kJ mol$^{-1}$, and is overall 27 kJ mol$^{-1}$ exothermic, forming **4d** by hydrogen-atom loss. Isomerization to the more stable ketyl radical **4b** is 65 kJ mol$^{-1}$ exothermic and overcomes a 17 kJ mol$^{-1}$ energy barrier in **TS4ab**. Radical **4b** does not lose the hydroxyl H atom directly but first undergoes isomerization by O−H bond rotation to **4c**. The O−H rotation is 19 kJ mol$^{-1}$ endothermic and requires overcoming a 22 kJ mol$^{-1}$ energy barrier in **TS4bc**. The O−H bond dissociation in **4c** is only 19 kJ mol$^{-1}$ endothermic but involves an energy barrier in **TS4cd** which is 70 kJ mol$^{-1}$ above **4c**.

The proximity of positive charge and hydrogen bonding to the OH group has an effect on the O−H bond dissociation energy, as studied for cation-radical **4e**$^{+\bullet}$ (Scheme 12). Table 3 data show that the O−H bond dissociation energy in **4e**$^{+\bullet}$ (17 kJ mol$^{-1}$) is similar to that in **4c** as judged by the threshold energies. However, the activation energy for O−H bond dissociation in **4e**$^{+\bullet}$ (**TS4ea**, 85 kJ mol$^{-1}$) is greater than that in **4c**, indicating a charge effect in the transition state.

**Model 5 Structures and Energetics.** The Gly−Gly−$NH_2$ system of model 5 allows for several structures of neutral molecules, cations formed by protonation, and radicals formed by electron capture reduction of the cations. Full conformational analysis of analogous peptide Gly−Gly−OH and (Gly−Gly−OH + $H^+$) systems has been reported recently,[38] and the most stable conformers reported there were taken as initial guesses for geometry optimizations in the present study. Protonation of the trans-isomer of Gly−Gly−$NH_2$ (**5c**) can occur at the N-terminal amine group or the Gly-2 carbonyl, giving rise to isomeric ammonium cations **5a**$^+$ and **5d**$^+$ or carbocations **5b**$^+$ and **5e**$^+$ (Scheme 13). Protonation at the Gly-1 carbonyl does not produce a stable cation; an attempted optimization resulted in spontaneous isomerization to structure **5e**$^+$ which shows the proton being chelated between the carbonyl oxygen atoms (Scheme 13). The N-terminus protonated cations show strong hydrogen bonding through a five-membered ring to the adjacent (Gly-2) carbonyl in **5a**$^+$, and through an eight-membered ring to the remote (Gly-1) carbonyl in **5d**$^+$. Ions **5a**$^+$, **5b**$^+$, and **5d**$^+$ are practically isoenergetic, while **5e**$^+$, a conformer of **5b**$^+$, is 31−36 kJ mol$^{-1}$ less stable (Table 4).

Electron capture reduction of **5a**$^+$−**5d**$^+$ results in substantial changes in the structures and relative energies of the formed radicals (Scheme 14). Electron capture in **5a**$^+$ forms a stable ammonium radical (**5a**) that shows an elongated and weakened

(38) Paisz, B.; Suhai, S. *Rapid Commun. Mass Spectrom.* **2001**, *15*, 2307−2323.

***Scheme 11***

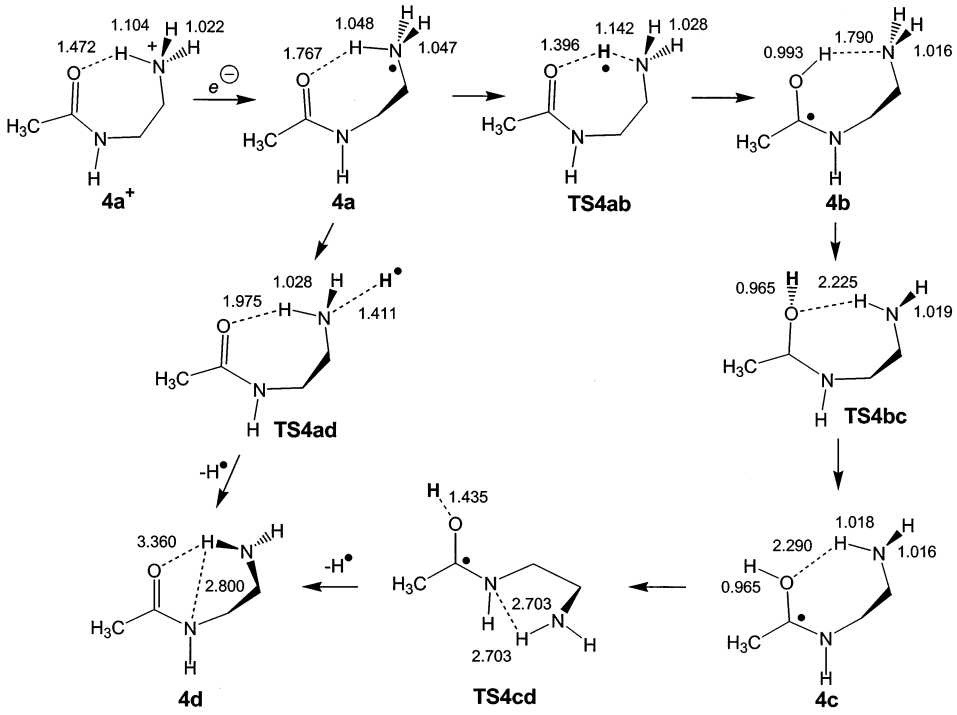


***Scheme 12***

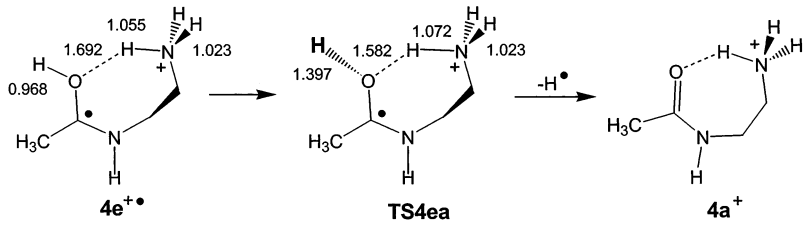


***Table 4.*** Energetics for Model 5 Cations and Radicals

| | relative energy[a] | | | |
|---|---|---|---|---|
| | 6-31++G(d,p) | 6-311++G(2d,p) | | |
| species/reaction | B3LYP | B3LYP | PMP2 | B3-PMP2 |
| **5a**$^+$ → **5c** + H$^+$ | | 933 | 926 | 930 (937)[b] |
| **5b**$^+$ → **5c** + H$^+$ | | 941 | 927 | 934 (941)[b] |
| **5d**$^+$ → **5c** + H$^+$ | | 928 | 930 | 929 (936)[b] |
| **5e**$^+$ → **5c** + H$^+$ | | 906 | 891 | 899 (905)[b] |
| **5a** → **5b** | −58 | −60 | −63 | −62 |
| **5a** → **TS5ab** | 15 | 14 | 25 | 19 |
| **5a** → **5c** + H$^•$ | −7 | −12 | −44 | −28 |
| **5a** → **TS5ac** | 13 | 12 | 12 | 12 |
| **5a** → **TS5ad** | 2 | 2 | 16 | 9 |
| **5a** → **5d** | −107 | −113 | −117 | −115 |
| **5d** → **5h** + $NH_3$ | −18 | −20 | −8 | −14 |
| **5b** → **5d** | −49 | −52 | −58 | −55 |
| **5b** → **5e** | 13 | 12 | 13 | 13 |
| **5b** → **5f** | 9 | 10 | 11 | 11 |
| **5b** → **5g** | 3 | 2 | 0.5 | 1 |

[a] 0 K relative energies in units of kJ mol$^{-1}$. [b] 298 K proton affinities.

hydrogen bond between the ammonium group and the Gly-2 carbonyl, which changes from 1.668 Å in **5a**$^+$ to 2.305 Å in **5a**. Likewise, radical **5b** has a substantially longer O−H···O hydrogen bond (1.822 Å) than has the corresponding cation **5b**$^+$ (1.423 Å). Electron capture in **5d**$^+$ does not result in a stable ammonium radical. Upon reduction, the out-of-plane $NH_3$ group spontaneously dissociates to form a dipole−dipole complex (**5d**), which is bound by hydrogen bonding between the $NH_3$ protons and the carbonyl oxygens (Scheme 14). Interestingly, and despite the N−C bond dissociation, complex **5d** is the most stable radical within the model 5 system (Table 4). The low energy of complex **5d** relative to the other model 5 radicals is likely due to the substantial stability of α-glycyl radicals.[39−43] Stabilization by hydrogen bonding of the ammonia molecule in **5d** amounts to only 12 kJ mol$^{-1}$ for dissociation forming a gauche-rotamer of the $^•CH_2CONHCH_2CONH_2$ radical which can further isomerize to the most stable anti-isomer **5h** (Scheme 14). Thermodynamically, **5d** is metastable with respect to exothermic dissociation to $NH_3$ and **5h** (Table 4).

Three other model 5 radicals were obtained as stable structures (Scheme 15). The Gly-2 ketyl radicals **5e** and **5f** are conformers of **5b**, of which **5f** is the most stable one. Note that **5f** has stabilizing hydrogen bonds between the ketyl OH and the N-terminus amine nitrogen (2.162 Å) and between the internal amide NH and the C-terminus carbonyl (2.209 Å). Finally, radical **5g** has a C-terminus ketyl OH group which is hydrogen bonded to the Gly-2 carbonyl at 1.810 Å (Scheme

(39) Yu, D.; Rauk, A.; Armstrong, D. A. *J. Am. Chem. Soc.* **1995**, *117*, 1789−1796.
(40) Bonifacic, M.; Stefanic, I.; Hug, G. L.; Armstrong, D. A.; Asmus, K.-D. *J. Am. Chem. Soc.* **1998**, *120*, 9930−9940.
(41) Tureček, F.; Carpenter, F. H.; Polce, M. J.; Wesdemiotis, C. *J. Am. Chem. Soc.* **1999**, *121*, 7955−7956.
(42) Ban, F.; Wetmore, S. D.; Boyd, R. J. *J. Phys. Chem. A* **1999**, *103*, 4303−4308.
(43) Carpenter, F. H.; Tureček, F. *J. Chem. Soc., Perkin Trans. 2* **1999**, 2315−2323.

***Scheme 13***

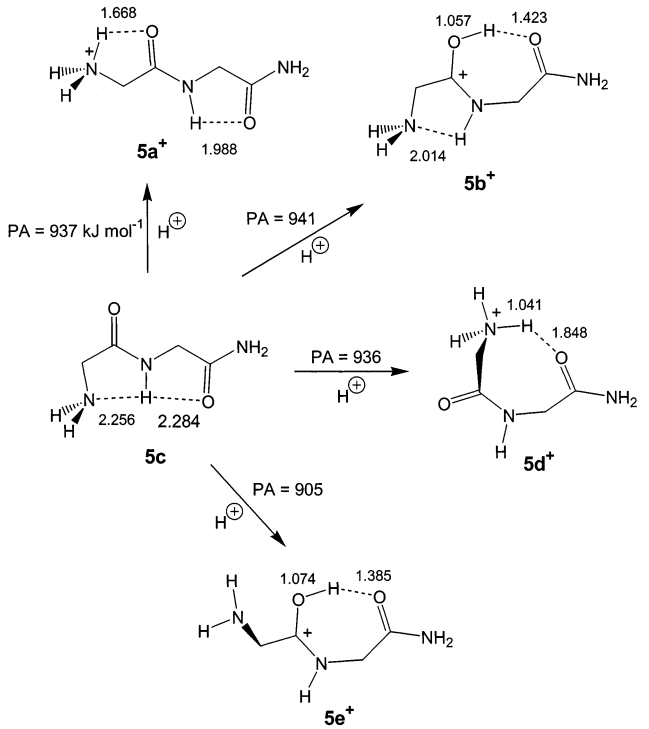


15). The ketyl radicals **5b**, **5e**, **5f**, and **5g** have similar energies which are within 13 kJ mol$^{-1}$ of each other, while **5a** is 49−62 kJ mol$^{-1}$ less stable (Table 4).

Hydrogen migration and dissociation was studied for **5a** and **5b**. An N−H bond break in the ammonium radical **5a** is 28 kJ mol$^{-1}$ exothermic but must overcome a 12 kJ mol$^{-1}$ energy barrier in **TS5ac** (Scheme 14). Ammonium H-atom migration to form **5b** requires a small barrier in **TS5ab** and is overall 62 kJ mol$^{-1}$ exothermic (Table 4). Transition states for the O−H bond breaks in **5b**−**5g** were also sought, but because of intramolecular hydrogen bonding in the reactants, gradient optimizations while stretching the O−H bond resulted in isomerization by hydrogen transfer. Although transition states for O−H bond dissociations undoubtedly exist in higher-energy radical conformers, a systematic search for such transition states would require detailed mapping of the radical conformational space, which is not feasible due to the size of these systems and the necessity of using spin unrestricted wave functions. By analogy with the systems of models 1−4, it can be reasonably assumed that the activation energies for direct O−H bond cleavages in **5b**−**5g** are in the 60−70 kJ mol$^{-1}$ range, which would make the direct cleavage competitive with the two step dissociation, for example, **5b** → **TS5ab** → **5a** → **TS5ac** → **5c** + H, requiring 79 kJ mol$^{-1}$ from **5b** to the highest **TS5ac** transition state.

Loss of $NH_3$ from **5a** is calculated to proceed through a low-lying TS (**TS5ad**, Scheme 14) which is only 9 kJ mol$^{-1}$ above **5a** (Table 4, B3-PMP2 value) and should be extremely facile. The departing $NH_3$ molecule can be weakly bound in complex **5d** (vide supra). However, because of the highly exothermic **5a** → **5d** isomerization, $-\Delta H_{rxn} = 115$ kJ mol$^{-1}$, complex **5d** is expected to rapidly dissociate when formed from **5a**. In addition to the very low activation energy, the loss of $NH_3$ has a positive activation entropy, $\Delta S^{\ddagger} = 11$ J mol$^{-1}$ K$^{-1}$ at 298 K, which facilitates dissociation.

**Excited Electronic States.** Electron capture in peptide ions is an exothermic process whose energy depends on the electronic state of the radical or cation-radical being formed. The upper bound for the internal energy acquired by electron capture is given by the pertinent adiabatic recombination energy (−RE) which is equal to the adiabatic ionization energy of the radical ($IE_a$). The $IE_a$'s for the systems of models 1−5 are summarized in Table 5. The ammonium radicals have $IE_a$'s in the 3.3−3.7 eV range, whereas the more stable ketyl radicals have an $IE_a$ = 4.0−4.75 eV. This shows that the $IE_a$ is mainly determined by the electronic properties of the functional group carrying the unpaired electron and less so by structure variations in the rest of the molecule. To extrapolate to larger, multiply charged, peptide cation-radicals, one needs to include the effect of remote positive charge that increases the recombination energy by Coulombic interaction. Presuming on average one positive charge per five amino acid residues in gas-phase cations with a $\beta$-sheet secondary structure and using a point charge model with the dielectric constant of vacuum, the increase of recombination energy is estimated at 0.8 eV per each nearest protonation site, and 0.4, 0.267, 0.2, 0.16, 0.133, 0.114, 0.10, 0.089, 0.080, 0.073, etc., eV for each more remote one. Hence, for example, the recombination energy for electron capture by the N-terminus ammonium group in a $(M + 10H^+)^{10+}$ peptide ion is estimated as 3.3 + 2.26 = 5.56 eV.

Because of low ionization energies, the peptide radicals have a dense manifold of closely spaced excited electronic states that can accept the incoming electron. Excited-state energies and radiative lifetimes were calculated for ammonium radicals **1a**, **4a**, and **5a** as shown in Table 6. The first five excited doublet states of ammonium radical **1a** (*A*−*E*) arise by promotion of the unpaired 25α electron to higher virtual orbitals. The CI matrix shows virtually no mixing of the doubly occupied orbitals (24α$\beta$ and lower) in the first five excited states (Table 6). The SOMOs in the *A*, *C*, *D*, and *E* excited states consist of diffuse orbitals of the Rydberg ns (26α, 28α) and np (29α, 30α) type. The SOMO in the *B* state (27α) is an antibonding $\pi$-type valence orbital. The *A*−*E* excited-state energies are within 1.75 eV of the ground *X* state. These low-lying excited states mostly show submicrosecond lifetimes for radiative transition to the ground state. Interestingly, the *A*−*E* states in **1a** are 1.3−0.3 eV lower in energy than the first (*A*) excited state of ketyl radical **1b** (Table 6). This means that, in contrast to ground-state isomerization **1a** → **1b** which is exothermic, isomerizations occurring on the potential energy surfaces of the low excited states of **1a** are endothermic and therefore disfavored by energy. Moreover, in the transition state for isomerization, **TS1ab**, the *A* state is very close to the ground-state surface with $\Delta E_{exc} = 0.71$ eV (Table 6). The *A* and *X* states also remain close in the TS for $NH_3$ loss, for example, $\Delta E_{exc} = 0.70$ eV in **TS1ah** (Table 6). This effect is analogous to the interaction of the *X* and *A* potential energy surfaces in other hypervalent "onium" radicals, for example, $(CH_3)_2NH_2^{\bullet}$[37e] and $(CH_3)_2OH^{\bullet}$,[44] where dissociations of the respective C−N and C−O bonds proceed through conical intersections of closely spaced *A* and *X* surfaces. As we discuss in the next section, the potential energy surface proximity in the transition states adversely affects Moller−Plesset calculations that show irregularities in the vicinity of the saddle points.

(44) Tureček, F.; Reid, P. J. *Int. J. Mass Spectrom.* **2003**, *222*, 49−61.

***Scheme 14***

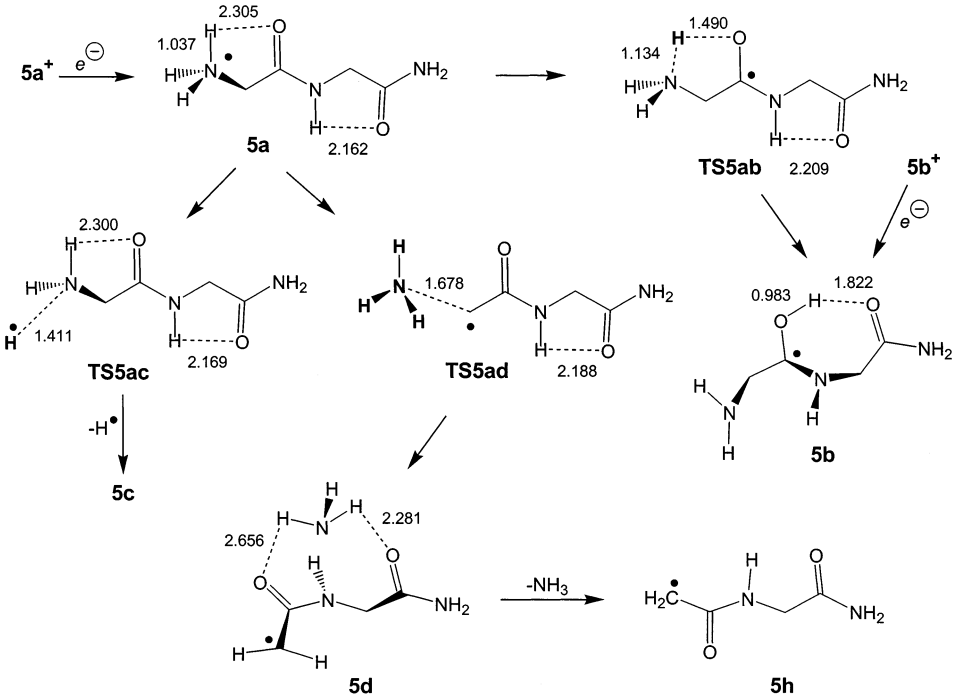


***Scheme 15***

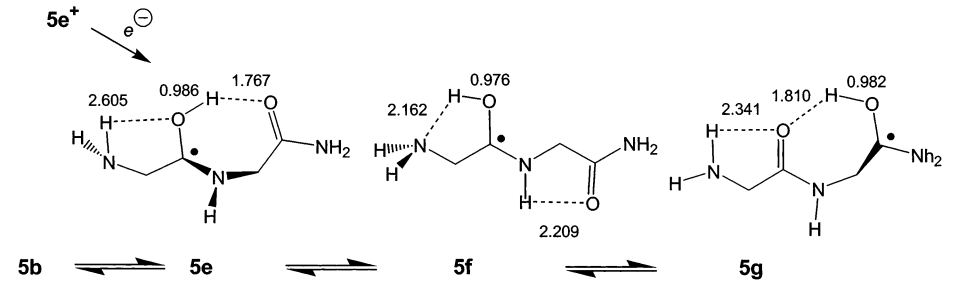


***Table 5.*** Proton Affinities and Ionization Energies

| species | proton affinity[a] | species | ionization energy[b] IE$_a$[c] | IE$_v$[d] | RE$_v$[e] |
|---|---|---|---|---|---|
| **1a**$^+$ → **1e** + H$^+$ | 955 (956)[f] | **1a** → **1a**$^+$ | 3.51 | 3.64 | 3.39 |
| **1c**$^+$ → **1f** + H$^+$ | 906 | **1d** → **1d**$^+$ | 4.10 | | 4.04 |
| **1d**$^+$ → **1f** + H$^+$ | 868 | **1d**$^+$ → **1j**$^{2+}$ | 10.93 | | |
| **1j**$^{+\bullet}$ → **1b** + H$^+$ | 940 (942)[f] | **Ie**$^+$ → **Ik**$^{2+}$ | 10.45 | | |
| **2a**$^+$ → **2c** + H$^+$ | 969 | **2a**$^\bullet$ → **2a**$^+$ | 3.40 | | |
| **3a**$^+$ → **3c** + H$^+$ | 968 | **3a**$^\bullet$ → **3a**$^+$ | 3.41 | | |
| **3d**$^+$ → **3f** + H$^+$ | 918 | **2d**$^\bullet$ → **2d**$^+$ | 4.01 | | |
| **2d**$^+$ → **2f** + H$^+$ | 913 | **2e**$^\bullet$ → **2e**$^+$ | 4.68 | | |
| **2e**$^+$ → **2f** + H$^+$ | 891 | **3e**$^\bullet$ → **3e**$^+$ | 4.75 | | |
| **3e**$^+$ → **3f** + H$^+$ | 895 | **4a** → **4a**$^+$ | 3.34 | | 3.13 |
| **4a**$^+$ → **4c** + H$^+$ | 974 (975)[f] | **4e**$^{+\bullet}$ → **4e**$^{2+}$ | 10.51 | | |
| **4e**$^{+\bullet}$ → **4b** + H$^+$ | 971 | **5a**$^\bullet$ → **5a**$^+$ | 3.71 | 3.85 | 2.77 |
| | | **5b**$^\bullet$ → **5b**$^+$ | 4.18 | 5.97 | 3.08 |
| | | [**5d**$^\bullet$] ← **5d**$^+$ | *g* | | 3.11 |
| | | **5e**$^\bullet$ → **5e**$^+$ | 4.54 | 6.02 | 3.35 |

[a] In units of kJ mol$^{-1}$ at 298 K. [b] In units of electronvolt (eV) at 0 K. [c] Adiabatic ionization energy. [d] Vertical ionization energy. [e] Vertical recombination energy taken as a positive value. [f] From effective QCISD(T)/6-311++G(2df,p) calculations. [g] Radical **5d** is not a stable structure.

Radicals **4a** and **5a** also show dense manifolds of excited electronic states (Table 6). Vertical excitation involves exclusively promotion of the odd electron from the SOMO to the virtual orbital space. The excitation energies depend on the ground-state geometry. Excitation from the optimized ($^2$A)*X* state of **5a** requires 1.14−1.56 eV to produce the *A*−*E* states. These have submicrosecond radiative lifetimes and can de-excited to the *X* state by photon emission. Excitation energies in vertically neutralized **5a** are lower, for example, 0.46−1.29 eV to reach the *A*−*E* states, indicating Franck−Condon effects upon electron capture and excitation.

The excited-state energies have important implications for energy deposition in and dissociation of peptide radicals produced by electron capture. If captured in a Rydberg orbital corresponding to an excited state of the radical, the electron can be de-excited to a lower electronic state by photon emission which carries away some of the energy due to ion−electron recombination. Energy can be conserved within the radical by internal conversion due to vibronic coupling of the electronic states. From the properties of ammonium radicals,[37e] it appears likely that N−H bond dissociations producing hydrogen atoms proceed from the *X* states, so that the excitation energies give estimates of the energy channeled into the dissociation. Although such an excitation would be irrelevant in dissociations of large protein cation-radicals, the extremely low activation energies for H-atom loss and migration would allow for fast reactions that are driven by the considerable thermal energy of the ion. The latter scales with the number of degrees of freedom in the ion.[45] Because the ion dissociations are observed on a time scale of seconds, the ions can get thermalized by blackbody radiation

(45) Tureček, F. *Org. Mass Spectrom.* **1991**, *26*, 1074−1081.

***Table 6.*** Electronic Excitation Energies and Radiative Lifetimes of th Radicals of Models 1, 4, and 5

| species | state | excitation energy (eV) | $f$ [a] | $\tau$ ($\mu$s)[b] | configuration |
|---|---|---|---|---|---|
| **1a**[c] | *A* | 0.77 | 0.011 | 3.6 | 0.35(25α → 26α) − 0.93(25α → 27α) |
| | *B* | 0.85 | 0.134 | 0.2 | 0.88(25α → 26α) + 0.27(25α → 27α) |
| | *C* | 1.21 | 0.130 | 0.1 | 0.78(25α → 28α) + 0.59(25α → 29α) |
| | *D* | 1.26 | 0.138 | 0.1 | 0.80(25α → 29α) − 0.56(25α → 28α) |
| | *E* | 1.74 | 0.076 | 0.1 | 0.81(25α → 30α) + 0.60(25α → 31α) |
| **TS1ab**[c] | *A* | 0.71 | 0.092 | 0.5 | 0.81(25α → 26α) − 0.11(25α → 27α) + 0.21(25α → 28α) |
| | *B* | 1.09 | 0.049 | 0.4 | 0.99(25α → 27α) + 0.18(25α → 28α) |
| | *C* | 1.22 | 0.135 | 0.1 | 0.18(25α → 27α) − 0.91(25α → 28α) + 0.31(25α → 29α) |
| | *D* | 1.34 | 0.109 | 0.1 | 0.26(25α → 28α) + 0.97(25α → 29α) |
| | *E* | 1.88 | 0.024 | 0.3 | 1.01(25α → 30α) + 0.21(25α → 31α) |
| **1b**[c] | *A* | 2.73 | 0.012 | 0.3 | 0.99(25α → 26α) + 0.12(25α → 27α) |
| | *B* | 3.05 | 0.030 | 0.1 | −0.12(25α → 26α) + 0.97(25α → 27α) + 0.21(25α → 29α) |
| | *C* | 3.40 | 0.034 | 0.06 | −0.16(25α → 27α) + 0.58(25α → 28α) + 0.79(25α → 29α) |
| | *D* | 3.44 | 0.012 | 0.2 | −0.15(25α → 27α) − 0.81(25α → 28α) + 0.56(25α → 29α) |
| | *E* | 4.04 | 0.015 | 0.1 | 0.95(25α → 30α) − 0.36(25α → 31α) |
| **TS1ah**[c] | *A* | 0.70 | 0.008 | 6.2 | 0.78(25α → 26α) + 0.56(25α → 27α) + 0.19(25α → 28α) |
| | *B* | 0.87 | 0.026 | 1.2 | −0.55(25α → 26α) + 0.81(25α → 27α) − 0.22(25α → 28α) |
| | *C* | 1.06 | 0.081 | 0.3 | −0.26(25α → 26α) + 0.94(25α → 28α) |
| | *D* | 1.44 | 0.102 | 0.1 | 0.89(25α → 29α) + 0.45(25α → 30α) |
| | *E* | 1.65 | 0.061 | 0.1 | 0.44(25α → 29α) + 0.87(25α → 30α) − 0.15(25α → 32α) |
| **1h**[c] | *A* | 4.44 | 0.001 | 0.8 | 0.85(20α → 21α) − 0.29(20α → 22α) − 0.13(20α → 23α) − 0.42(19$\beta$ → 20$\beta$) |
| | *B* | 4.46 | 0.003 | 0.4 | 0.39(20α → 21α) − 0.13(20α → 22α) + 0.91(19$\beta$ → 20$\beta$) |
| | *C* | 4.71 | 0.002 | 0.5 | composite α, $\beta$ |
| | *D* | 5.06 | 0.009 | 0.1 | composite α, $\beta$ |
| | *E* | 5.12 | 0.002 | 0.5 | composite α, $\beta$ |
| **4a**[c] | *A* | 0.66 | 0.069 | 0.8 | 29α → 30α |
| | *B* | 0.83 | 0.044 | 0.8 | 29α → 31α |
| | *C* | 1.04 | 0.19 | 0.1 | 29α → 32α |
| | *D* | 1.20 | 0.12 | 0.1 | 29α → 33α |
| | *E* | 1.55 | 0.018 | 0.5 | 29α → 34α |
| **4a** (VN)[d] | *A* | 0.47 | 0.017 | | 29α → 0.55(30α) + 0.84(31α) |
| | *B* | 0.66 | 0.12 | | 29α → 0.44(31α) − 0.71(30α) |
| | *C* | 0.95 | 0.19 | | 29α → 32α |
| | *D* | 1.08 | 0.14 | | 29α → 33α |
| | *E* | 1.39 | 0.028 | | 29α → 34α |
| **4b**[c] | *A* | 2.34 | 0.009 | 0.5 | 29α → 30α |
| | *B* | 2.68 | 0.010 | 0.01 | 29α → 31α |
| | *C* | 3.01 | 0.023 | 0.1 | 29α → 0.53(32α) − 0.83(33α) |
| | *D* | 3.04 | 0.041 | 0.06 | 29α → 0.84(32α) + 0.51(33α) |
| | *E* | 3.51 | 0.003 | 0.7 | 29α → 34α |
| **5a**[c] | *A* | 1.14 | 0.066 | 0.3 | 36α → 37,38,39,41α mixed state |
| | *B* | 1.24 | 0.037 | 0.4 | 36α → 37α |
| | *C* | 1.38 | 0.092 | 0.1 | 36α → 38,39,40,41α mixed state |
| | *D* | 1.44 | 0.068 | 0.2 | 36α → 38,39,40,41α mixed state |
| | *E* | 1.56 | 0.17 | 0.06 | 36α → 40α |
| **5a** (VN)[d] | *A* | 0.46 | 0.005 | | 36α → 38,39,41α mixed state |
| | *B* | 0.61 | 0.038 | | 36α → 37α |
| | *C* | 0.71 | 0.012 | | 36α → 38,39α mixed state |
| | *D* | 1.07 | 0.080 | | 36α → 40α |
| | *E* | 1.29 | 0.22 | | 36α → 41α |

[a] Oscillator strength. [b] Radiative lifetimes for transitions to the doublet *X* state. [c] Vertical excitations from optimized geometries of radical ground doublet states. [d] Excitation energies in radicals formed by vertical electron capture in the corresponding cations.

that occurs on a comparable time scale, and the rate of thermalization increases with the ion size.[46] This implies that low-activation energy reactions by H loss or migration will occur regardless of the ion size on a time scale which is much shorter than those determined by the experimental setup.

**Dissociation and Recapture Kinetics.** The calculated activation energies indicate that dissociations of peptide ammonium radicals relevant to ECD can occur by competing H-atom loss from the ammonium group, H-atom transfer to an acceptor carbonyl group, or loss of ammonia. The kinetics of these dissociations depend on experimental conditions that determine the energy transfer between the reactants and the surrounding medium. For dissociations of isolated radicals that are observed on a short time scale, the RRKM model is appropriate for treating the kinetics. In contrast, radicals that are trapped in an ICR cell for a long time can exchange energy with the environment by radiative heating or cooling.[46] Hence, the dissociation kinetics of long-lived species can be treated by the transition state theory (TST) as if the radicals had Boltzmann distribution of internal energies.[46] The rate-limiting process can be the thermalization or dissociation, whichever is slower.

Because of the generally low energy barriers for exothermic loss or transfer of ammonium hydrogen, the rate constants for these reactions are subject to tunneling corrections.[47] A rigorous treatment of tunneling effects requires dealing with multidimensional potential energy surfaces (PES) to account for barrier penetration along vectors transversal to the reaction coordinate (e.g., the corner cutting and bobsledding effects).[48] Following

(46) Price, W. D.; Schnier, P. D.; Jockusch, R. A.; Strittmatter, E. F.; Williams, E. R. *J. Am. Chem. Soc.* **1996**, *118*, 10640−10644.

(47) Bell, R. P. *The Tunnel Effect in Chemistry*; Chapman and Hall: London, 1980; p 27.

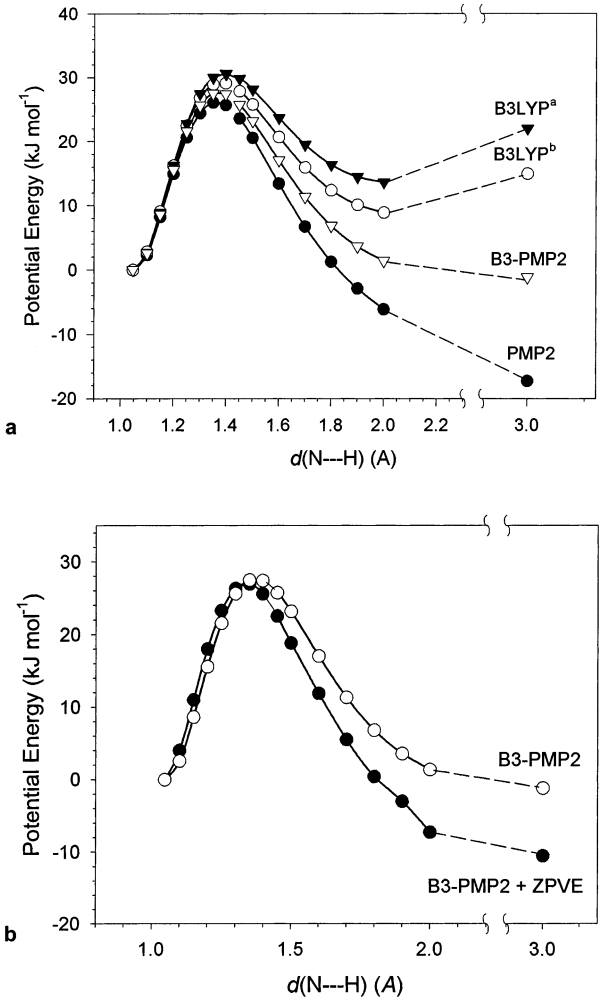


***Figure 1.*** Top: Potential energy surface for N−H bond dissociation in **1a**. ▼, B3LYP/6-31++G(d,p) energies; ○, B3LYP/6-311++G(2df,p) energies; ●, PMP2/6-311++G(2df,p) energies; ▽, B3-PMP2/6-311++G-(2df,p) energies. Bottom: B3-PMP2 (○) and ZPVE-corrected B3-PMP2 (●) potential energy surfaces.

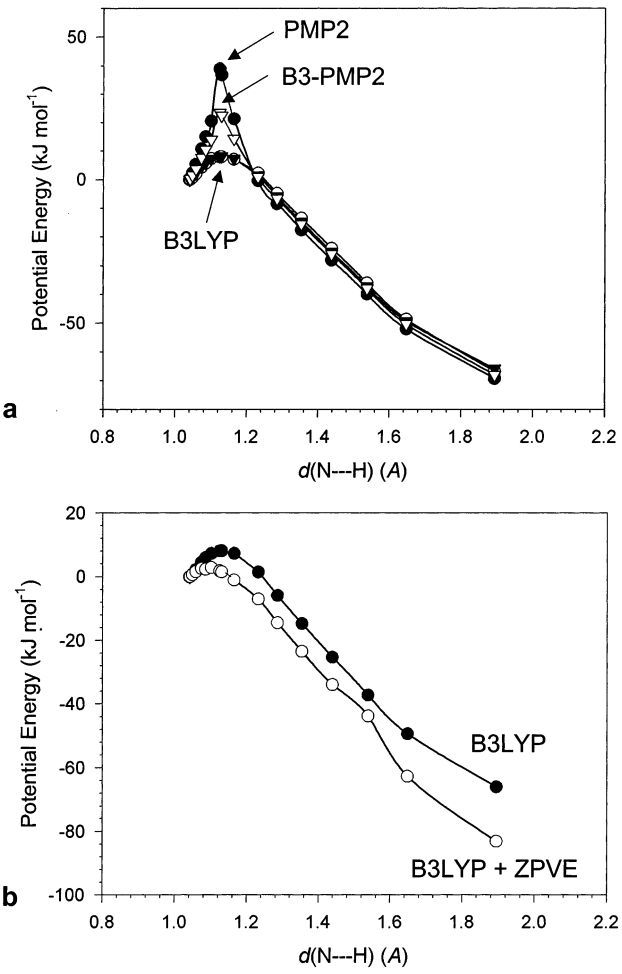


***Figure 2.*** Top: Potential energy surface for N−H→O migration in **1a**. ▼, B3LYP/6-31++G(d,p) energies; ○, B3LYP/6-311++G(2df,p) energies; ●, PMP2/6-311++G(2df,p) energies; ▽, B3-PMP2/6-311++G(2df,p) energies. Bottom: B3LYP (●) and ZPVE-corrected B3LYP (○) potential energy surfaces.

a simplified one-dimensional approach,[49] we obtained potential energy profiles by stepwise single-point calculations at several points along the reaction coordinates. The PES were corrected for zero-point energies from vibrational modes transversal to that representing the reaction coordinate which was identified by visual mode inspection and confirmed by intrinsic reaction coordinate (IRC) calculations.[50] The choice of the potential energy surface turned out to be critical, because both B3LYP and MP2 surfaces showed deficiencies. For N−H bond dissociations, the B3LYP PES gave reasonable TS energies (Table 1), but showed false minima at N···H separations >2 Å followed by an energy increase on the way to the products (Figure 1, top). In contrast, the B3-PMP2 PES gives a good match with the stationary points calculated by effective QCISD(T)/6-311++G(2df,p) for **1a**, **TS1ae**, and **1e** + H, and so the ZPVE-corrected B3-PMP2 PES (Figure 1, bottom) was used to calculate tunneling effects for all N−H bond dissociations. The PES for dissociations of **2a**, **4a**, and **5a** showed analogous properties and are given in the Supporting Information.

For the N···H···O migration in **1a**, the PES from MP2 single-point calculations showed incorrect curvature in the vicinity of the saddle points (Figure 2, top). This was probably caused by mixing of closely spaced excited electronic states (see above) in the perturbational energy treatment. Interestingly, similar effects were observed for QCISD(T) single-point calculations that also showed very high energies for the TS (Table 1).

In contrast, the B3LYP calculations gave regular PES shapes, and, following ZPVE correction, the B3LYP/6-311++G(2df,p) surface was used to calculate tunneling effects for the N−H→O migration in **1a** (Figure 2, bottom).

The PMP2 PES for C−$NH_3$ bond cleavage in **1a** also showed a cusp in the vicinity of **TS1ah** (Figure 3, top), while the B3LYP PES had correct energy gradients. The ZPVE-corrected B3LYP/6-311++G(2df,p) PES (Figure 3, bottom) was used for calculations of tunneling corrections.

The barriers for dissociations and isomerizations **2a**, **4a**, and **5a** were quite analogous (Supporting Information, Figures S1−S12) and were treated in the same manner as those for **1a**.

Permeabilities ($G(E)$) were calculated for Eckart barriers[51] that were fitted to the ZPVE-corrected PES such as to best

(48) Fernandez-Ramos, A.; Truhlar, D. G. *J. Chem. Phys.* **2001**, *114*, 1491−1496.
(49) Truhlar, D. G.; Kuppermann, A. *J. Am. Chem. Soc.* **1971**, *93*, 1840−1851.
(50) Gonzalez, C.; Schlegel, H. B. *J. Phys. Chem.* **1990**, *94*, 5523−5527.
(51) Eckart, C. *Phys. Rev.* **1930**, *35*, 1303.

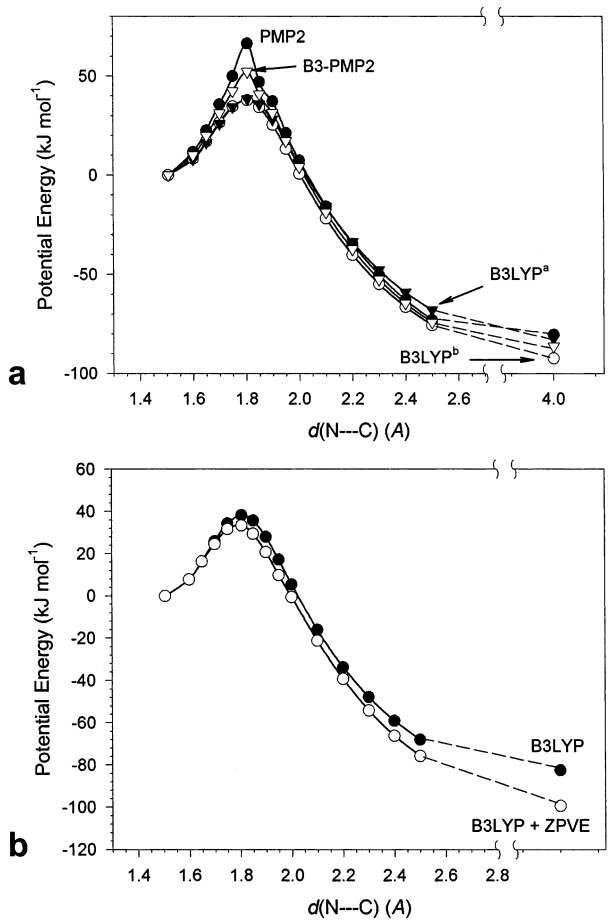


***Figure 3.*** Top: Potential energy surface for C−$NH_3$ bond dissociation in **1a**. ▼, B3LYP/6-31++G(d,p) energies; ○, B3LYP/6-311++G(2df,p) energies; ●, PMP2/6-311++G(2df,p) energies; ▽, B3-PMP2/6-311++G-(2df,p) energies. Bottom: B3LYP (●) and ZPVE-corrected B3LYP (○) potential energy surfaces.

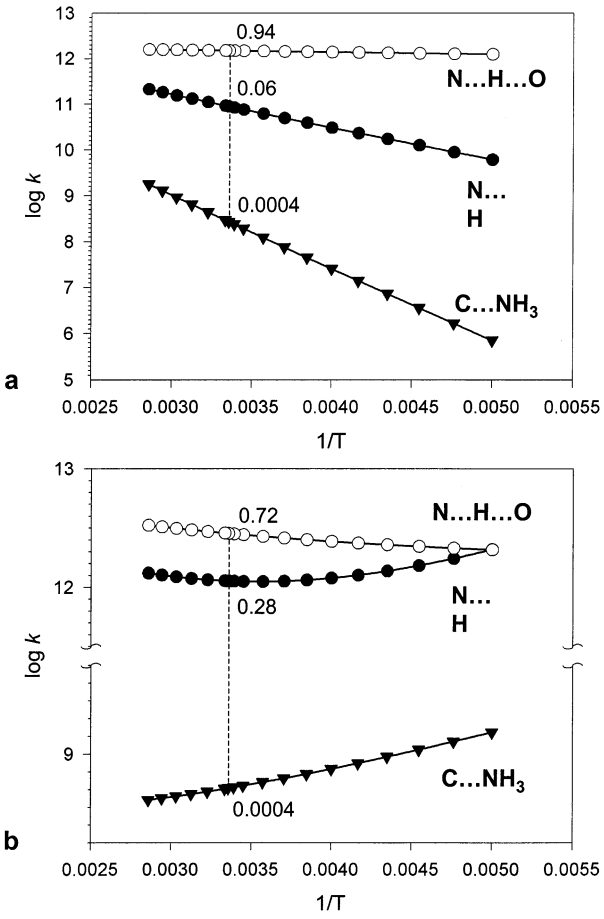


***Figure 4.*** (a) TST rate constants (log *k*) for dissociations and isomerizations of **1a**. (b) Rate constants (log *k*) with tunneling corrections. The vertical dashed lines are drawn at 298 K, and the numbers indicate the 298 K branching ratios.

reproduce the barrier widths at all points. As discussed by Truhlar and Kuppermann,[49] Eckart functions may not reproduce the exact PES shape. However, because the permeability depends only on the barrier width at any given energy, matching the widths and the barrier height is sufficient for reliable $G(E)$ calculations. This was carried out for the N−H bond cleavages (Figure S13, S16, S18, and S20, Supporting Information), N- -H- -O migrations (Figure S14, S17, S19, and S21, Supporting Information) in **1a**, **2a**, **4a**, and **5a**, and C−$NH_3$ bond dissociation (Figure S15, Supporting Information) in **1a**, where the Eckart functions (dashed lines) were replotted (solid lines) to visualize how their widths compare with those of the ZPVE-corrected PES. The calculated $G(E)$ values were convoluted with Boltzmann energy distribution according to eq 1 to give the tunneling correction factor ($\kappa$),[51] where $E_a$ is the activation energy, and $k_B$ is the Boltzmann constant.

$$\kappa = e^{E_a/k_BT} \int_0^\infty G(E) e^{-E/k_BT} d\left(\frac{E}{k_BT}\right) \qquad (1)$$

To compare the kinetics of radical dissociations through competing channels, it was mandatory to use a consistent set of activation energies for TST calculations. Because of the difficulties with MP2 TS energies (see above) that also affected the B3-PMP2 values, we used ZPVE-corrected B3LYP/6-311++G(2df,p) TS energies to obtain TST rate constants. The TST and tunneling-corrected rate constants are plotted as log *k* against 1/*T* for the dissociations of the radicals of models 1, 2, 4, and 5. Figure 4 indicates very fast dissociation of **1a** through **TS1ae** and isomerization through **TS1ab**, with 298 K rate constants of log $k \geq 11$. By contrast, loss of $NH_3$ which is 2−3 orders of magnitude slower is not expected to compete efficiently with the H loss and migration. Tunneling effects cause substantial curvature in the Arrhenius plots (Figure 4b) but do not alter the ordering of rate constants, $k$(H migration) > $k$(H loss) > $k$($NH_3$ loss), except for very low temperatures. The 298 K branching ratios for $k$(H migration)/$k$(H loss) are 0.94:0.06 and 0.72:0.28 without and with tunneling corrections, respectively (Figure 4).

The inverted Arrhenius plot for $NH_3$ loss in Figure 4b is due to heavy atom tunneling analogous to that reported by Carpenter for isomerization in cyclobutadiene.[52] The 298 K tunneling correction was $\kappa = 2.4$ for the C−$NH_3$ bond dissociation in **1a**.

H-atom loss from and migration in **2a** are also fast and competitive. Figure 5a shows a $k$(H migration)/$k$(H loss) branching ratio of 0.64:0.36 when based on TST rate constants. This is reversed to 0.21:0.79 when including tunnel corrections (Figure 5b). In contrast, H-atom migration in **4a** was found to be consistently faster than N−H bond dissociation regardless

(52) Carpenter, B. K. *J. Am. Chem. Soc.* **1983**, *105*, 1700−1701.

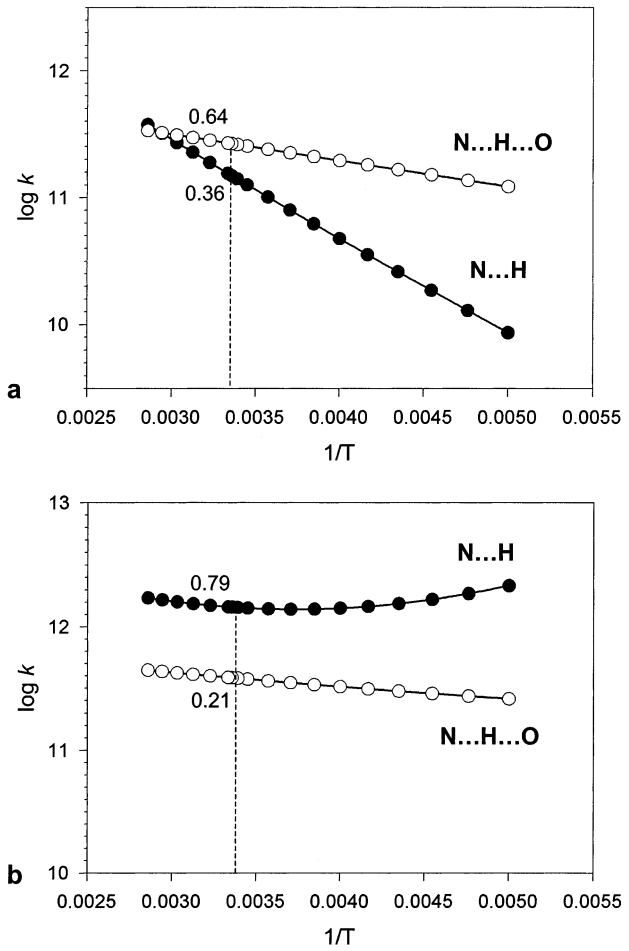


***Figure 5.*** (a) TST rate constants (log *k*) for dissociations and isomerizations of **2a**. (b) Rate constants (log *k*) with tunneling corrections. The vertical dashed lines are drawn at 298 K, and the numbers indicate the 298 K branching ratios.

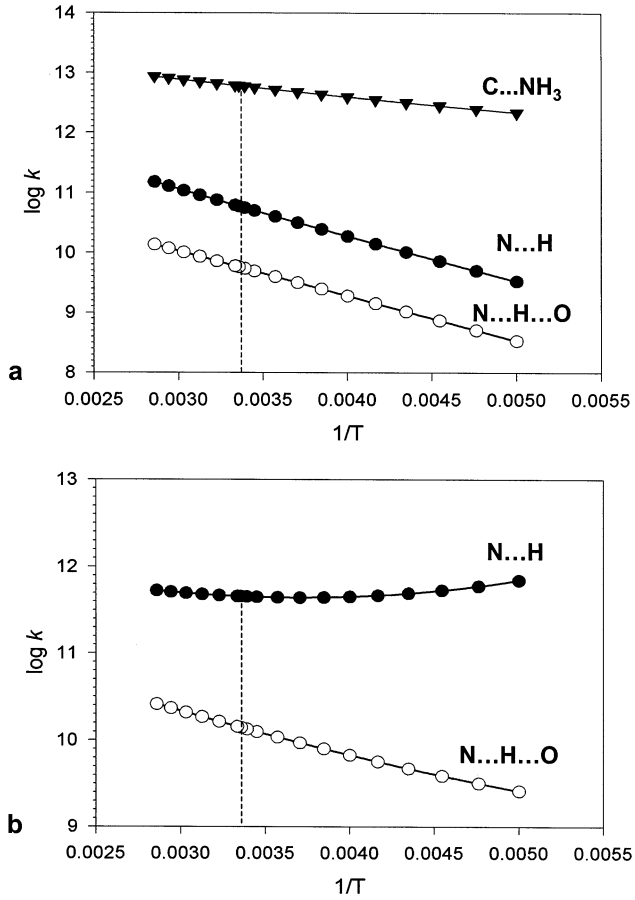


***Figure 6.*** (a) TST rate constants (log *k*) for dissociations and isomerizations of **5a**. (b) Rate constants (log *k*) with tunneling corrections. The vertical dashed lines are drawn at 298 K.

of tunneling effects and gave *k*(H migration)/*k*(H loss) = 0.81:0.19 at 298 K, showing a very shallow dependence on temperature (Figure S22). Both rate constants point to very fast dissociation of **4a** with log $k > 11.5$ over the entire temperature range. The rate constants for **5a** dissociations (Figure 6a) show dominant loss of $NH_3$ of log $k_{298} = 12.8$. Regardless of tunneling, the loss of H is an order of magnitude faster than the N−H→O migration (Figure 6b).

The difference in the relative rates for the N−H→O migration in **1a**, **2a**, **4a**, and **5a** can be explained by steric and ring size effects in the TS. The migration is most favorable when proceeding through a seven-membered **TS4ab**, which allows the best alignment of the N−H−O atoms and the closest O··H approach (Scheme 11). In contrast, the five-membered **TS5ab** involves both a ring strain and the least favorable O··H approach and as a result has the highest TS energy of the H migrations. The six-membered **TS2ab** and **TS3ab** probably include small steric interactions between the *N*-methyl group and the ring atoms which are absent in **TS1ab**.

The previous kinetic analysis showed that H-atom transfer and loss are in competition in dissociations of ammonium radicals **1a**, **2a**, **4a**, and **5a**. To be important for ECD-like dissociations, the hydrogen atom released from the ammonium group must be recaptured by an acceptor amide group. H-atom additions to amide carbonyl groups must overcome substantial activation barriers, for example, 42, 57, 38, 48, and 68 kJ mol$^{-1}$ for additions to **1f**, **1a**$^+$, **3f**, **4d**, and **4a**$^+$, respectively.[53] The barriers cause the rate constants for capture of a *thermal* hydrogen atom to be very small, for example, $k_{298} = 3.2 \times 10^{-18}$ molecule cm$^{-3}$ s$^{-1}$ in **3f**, and yet smaller in the other amides. Even if the addition rate is enhanced by ∼1 order of magnitude by tunneling through the potential energy barrier, the thermal rate constants are too small to make the recapture competitive.

An increased reaction rate can also occur for capture of *translationally hot* H atoms released by exothermic dissociation of the ammonium radical. Reactions of hot atoms of high (>100 eV) kinetic energies can be treated using the Estrup−Wolfgang kinetic model that uses the energy-dependent collision probability, $p(E)$, and the reaction energy window as the critical parameters.[54] Unfortunately, $p(E)$ values are not available from first-principle calculations. For hyperthermal hydrogen atoms of kinetic energies ≤3 eV, one can assume near-equilibrium conditions in the reactant molecule and adjust the capture rate constant according to eq 2 derived from Keizer's steady-state theory,[55] where $T^*$ is the hot H-atom translational temperature calculated from its kinetic energy ($T^* = 2E_{hot}/3k_B$), $T$ is the

(53) The B3-PMP2 barriers for H-atom addition to the amide groups are consistent with those calculated for addition to formamide (51 kJ mol$^{-1}$ by CCSD(T)/aug-cc-pVTZ, ref 15) and *N*-methylacetamide (53 kJ mol$^{-1}$ by G2, ref 16).
(54) Estrup, P. J.; Wolfgang, R. *J. Am. Chem. Soc.* **1960**, *82*, 2665−2669.
(55) Keizer, J. *J. Chem. Phys.* **1973**, *58*, 4524−4535. For a review, see: Gaspar, P. P.; Root, J. W. *Radiochim. Acta* **1981**, *28*, 191−213.

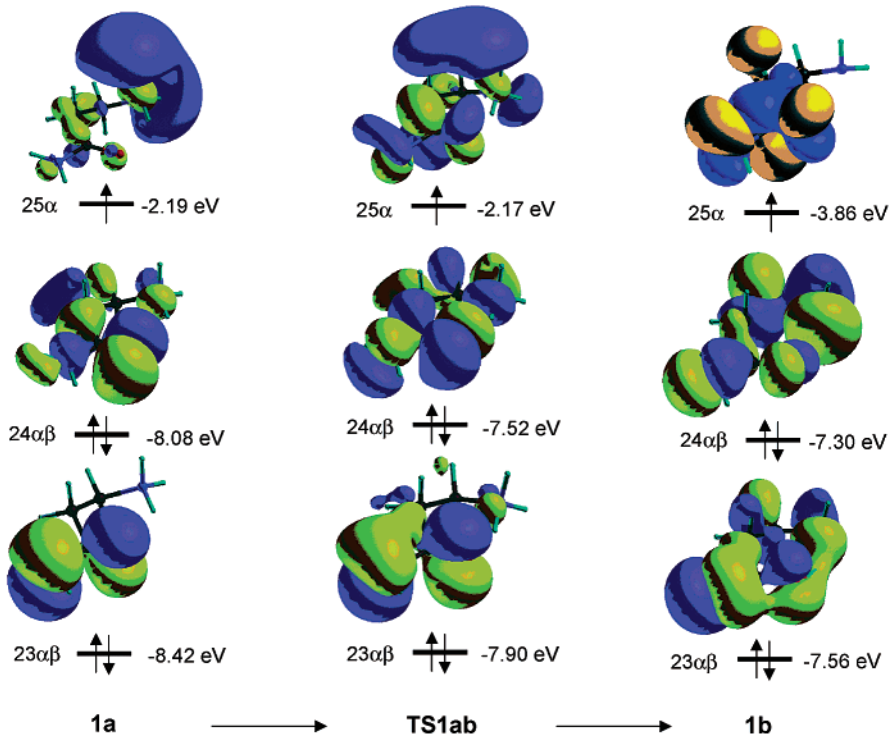


***Figure 7.*** Frontier orbital depiction of H-atom migration in **1a**. Singly occupied molecular orbitals are denoted as $n\alpha$; doubly occupied orbitals are denoted as $n\alpha\beta$. The orbital energies are from B3LYP/6-311++G(2d,p) calculations relative to the ionization limit.

temperature of the peptide, and $\sigma^*$ and $\sigma$ are the cross sections for the capture of hot and thermal hydrogen atoms, respectively.

$$\frac{k_{\text{hot}}}{k_{\text{thermal}}} = \left(\frac{T}{T^*}\right)^{3/2} \frac{\int_{E_a}^{\infty} \sigma^*(E) E e^{-E/k_B T^*}\, dE}{\int_{E_a}^{\infty} \sigma(E) E e^{-E/k_B T}\, dE} \qquad (2)$$

Under a zero-order approximation of energy-independent $\sigma$, $\sigma^*(E) = \sigma(E) =$ constant, integration of eq 2 gives eq 3, which indicates a substantial acceleration in the capture of hot atoms.

$$\frac{k_{\text{hot}}}{k_{\text{thermal}}} = \sqrt{\frac{T^*}{T}} \times \frac{e^{-E_a/k_B T^*}\left(1 + \frac{E_a}{k_B T^*}\right)}{e^{-E_a/k_B T}\left(1 + \frac{E_a}{k_B T}\right)} \qquad (3)$$

For a hydrogen atom that has been accelerated to a 100 kJ mol$^{-1}$ translational energy due to exothermic dissociation, eq 3 gives $k_{\text{hot}}/k_{\text{thermal}} \approx 1.3 \times 10^6$ for addition to **3f**. This acceleration brings the recapture rate constant to $4.2 \times 10^{-12}$ molecule cm$^{-3}$ s$^{-1}$, which is within the typical range of rate constants for proton-transfer reactions in the gas phase.[56] Considering that the hydrogen atom is produced intramolecularly from an ammonium radical precursor, we find that the reaction volume is confined to the molecular volume of $10^{-20}$–$10^{-22}$ cm$^3$. Hence, the pseudounimolecular rate constants for H-atom addition are on the order of $10^8$–$10^{10}$ s$^{-1}$ and make the H-atom recapture competitive with direct N–H→O transfer.

**Electronic Properties of Radicals and Transition States.** The calculated rate constants for N–H bond cleavage and N–H→O migration show unambiguously that the latter reaction should occur competitively in the ammonium radicals under study. The pertinent energy barriers for both reactions show dependence on the reactant structure. Cleavage of the out-of-plane ammonium N–H bond is most facile in **4a** and **TS4ad**, which have the strongest hydrogen bonds mediated by the nondissociating, in-plane proton, as indicated by the O–H distances ($d_{\text{O–H}}$), which are $d_{\text{O–H}}$ =1.767 and 1.975 Å in **4a** and **TS4ad**, respectively. The TS energy increases with decreasing hydrogen bonding, for example, in **2a** ($d_{\text{O–H}}$ = 1.924 Å) and **5a** ($d_{\text{O–H}}$ = 2.305 Å). The energy barriers for N–H→O migration follow the same trend, which is intuitively obvious, as the shortest H···O approach in **4a** is expected to result in the lowest activation energy in **TS4ab**. It should be noted, however, that the lengths of the dissociating N–H bond in the transition states for H-atom loss are very similar for the radicals of models 1–5 (1.398–1.411 Å, Schemes 3–15).

The radical and transition state geometries and energies can be explained or interpreted by analyzing the pertinent molecular orbitals, atomic charges, and spin distributions in the reactants and their changes during the reactions. A common feature of ammonium radicals **1a**–**5a** is that they all have high-lying singly occupied molecular orbitals (SOMO) of a ns (Rydberg) type that are delocalized over the out-of-plane ammonium hydrogens (Figures 7 and 8) which carry most of the spin density. In contrast, the in-plane, hydrogen-bonded, hydrogen atoms are situated in the nodal plane of the SOMOs and have negligible spin density (Schemes 16 and 17). The electron distribution is further illustrated by the atomic charge densities that show net negative charge at the out-of-plane ammonium hydrogens, whereas the in-plane hydrogen has a positive charge and can be best represented as an ammonium proton. The presence of substantial negative charge within the radical ammonium group

(56) (a) Bohme, D. K.; Mackay, G. I.; Schiff, H. I. *J. Chem. Phys.* **1980**, *73*, 4976–4986. (b) Lias, S. G.; Shold, D. M.; Ausloos, P. *J. Am. Chem. Soc.* **1980**, *102*, 2540–2548.

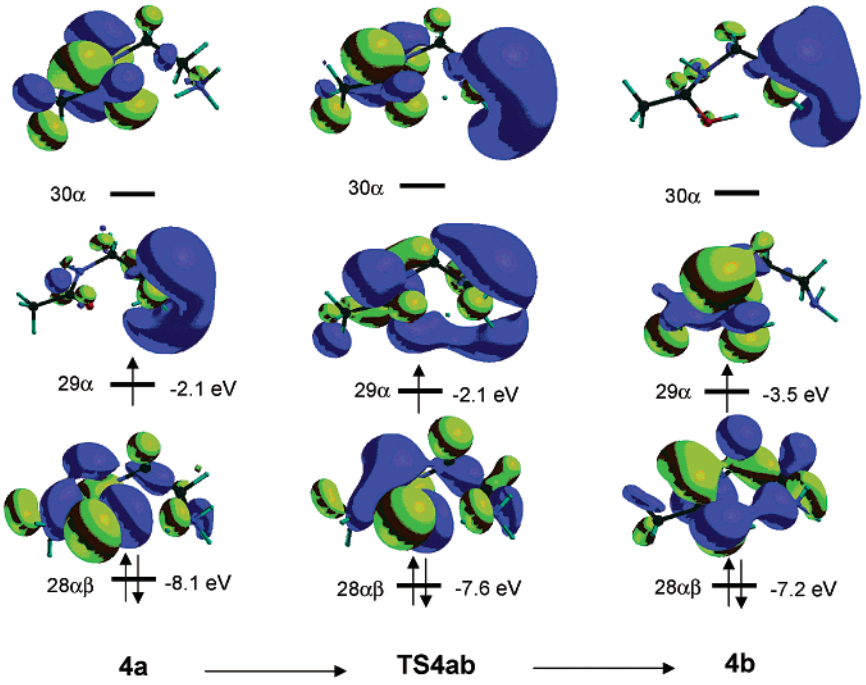


***Figure 8.*** Frontier orbital depiction of H-atom migration in **4a**. Singly occupied molecular orbitals are denoted by *n*α; doubly occupied orbitals are denoted by *n*α*β*. The orbital energies are from B3LYP/6-311++G(2d,p) calculations relative to the ionization limit.

***Scheme 16***

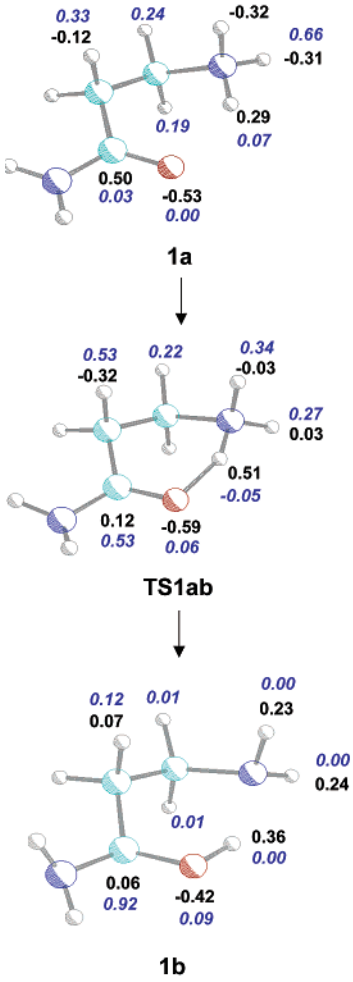


***Scheme 17***

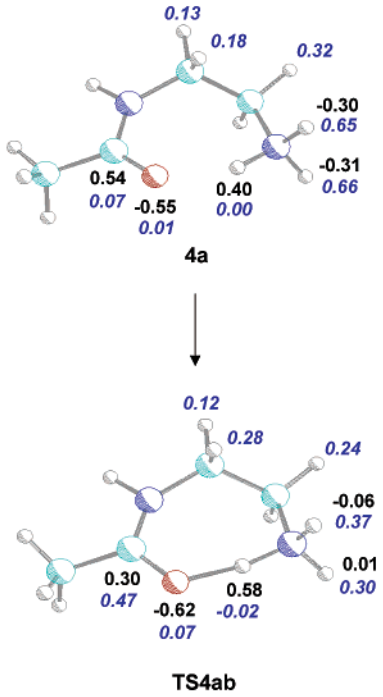


explains the weakening of hydrogen bonding upon electron capture. This is essentially a Coulombic effect due to the repulsion of the negatively charged carbonyl oxygen and the out-of plane ammonium hydrogens. The charge and spin distributions change in the course of N−H→O migration in a fashion that depends on the radical structure. In model 1 radicals, the in-plane H atom migrates in a clockwise fashion through a six-membered cyclic transition state (Scheme 16). The atomic charges are shown as bold black numerals; the spin densities are shown as bold italic blue numerals. The migrating H atom has a positive charge in the reactant **1a** (+0.29) that increases in **TS1ab** (+0.51) and then decreases in the ketyl product **1b** (+0.36). Simultaneously, the migrating H atom has a very low spin density throughout the reaction. The negative charge density

in **1a** is to a large part localized in the out-of-plane ammonium hydrogen atoms which also carry most of the spin density in **1a**. In **TS1ab**, the electron density flows from the out-of-plane ammonium hydrogens to the methylene hydrogen atoms and the carbonyl carbon atom, which both gain substantial spin density. Note that while the clockwise proton motion indicates an early transition state for **TS1ab** resembling the reactant **1a**, the counterclockwise electron reorganization is more advanced in **TS1ab** where the charge and spin densities resemble those in the ketyl product **1b**.

The latter shows positively charged amine hydrogens (+0.23) and a virtually electroneutral ketyl carbon atom. The low charge density on the latter results from the negative charge contribution from the SOMO $\pi$-orbital that carries most of the spin density (0.92) in **1b** and the $\sigma$-electron-withdrawing effect of the amide O and N atoms.

The electron reorganization in **1a** → **TS1ab** → **1b** is equivalently depicted by the frontier orbitals shown in Figure 7. The SOMO in **1a** is a diffuse orbital delocalized over the out-of-plane ammonium hydrogens, whereas the in-plane proton is in the region of negligible SOMO density. In the TS, the SOMO mixes in the pseudo-$\pi$ orbitals of the bridge methylene groups to eventually become the carbon-centered $\pi$-orbital in the ketyl product **1b**.

A somewhat different course of electron reorganization is calculated for the isomerization **4a** → **TS4ab** → **4b**, where the hydrogen motion is shown as proceeding in a clockwise direction (Scheme 17). The migrating in-plane ammonium hydrogen starts with a positive charge (+0.40) in **4a** and becomes more positive in **TS4ab** (+0.58), indicating again proton migration. Accordingly, the migrating proton has negligible spin density throughout the reaction. The electron reorganization is best viewed by spin density changes. Radical **4a** has most of the spin density delocalized over the out-of plane ammonium and methylene hydrogen atoms (Scheme 17). In the TS, the spin density at the ammonium and adjacent methylene hydrogens decreases, and spin flow goes to the incipient ketyl carbon and one of the $N-CH_2$ methylene hydrogens. Note that the amide nitrogen atom, which is in the counterclockwise path for electron flow, does not acquire any spin density in the course of the reaction. In the product **4b**, the spin density is mostly localized at the ketyl carbon (0.92) with some delocalization over the adjacent methyl group (0.1).

The frontier molecular orbitals show a spatial representation of the electron reorganization in **4a** (Figure 8). The SOMO in **4a** is a diffuse ns-type orbital that mostly includes the out-of-plane ammonium hydrogens. In **TS4ab**, the SOMO develops lobes over the methylene groups and the ketyl carbon atom, but there is a nodal plane at the amide nitrogen atom which interrupts the electron flow in the counterclockwise direction. The migrating proton moves clockwise in the SOMO nodal space. Because of the "insulating" effect of the amide nitrogen, the overall electron flow can be viewed as clockwise, in the same sense as the migrating proton motion.

In summarizing the electronic description of H-atom migrations in the radicals of models 1−5, the proton and electron motions are decoupled in time and space. For the systems under study, the nuclear motion indicates early transition states that resemble the reactants. In contrast, the electron distribution in the TS indicates substantial charge and spin density flow on the way to the products. The space separation is obvious from the orbital shapes. While the proton migrates close to the plane defined by the cyclic five- to seven-membered transition state geometry, the electron flow occurs through out-of-plane $\pi$-type orbitals that sandwich the migration plane in which they have the node.

## Conclusions

The present calculations indicate that H-atom loss and migration in hypervalent ammonium radicals produced by electron capture are very fast reactions when occurring in isolated or thermalized gas-phase radicals. With the model amide and peptide radicals studied here, large tunneling effects make the migration of ammonium H competitive with its loss. The migration can be described by the proton-coupled electron transfer model[22−24] in which the nuclear (proton) and electronic reorganizations are partially decoupled in time and completely decoupled in space. The time decoupling manifests itself by the electron reorganization preceding the nuclear motion. The space decoupling results in the proton and electron moving in separate regions of space and in the same or opposite direction, depending on the electronic properties of the chain connecting the ammonium and amide groups.

**Acknowledgment.** This paper is dedicated to Professor Fred W. McLafferty on the occasion of his 80th birthday. Support of this work by NSF (Grants CHE-0090930 for experimental work and CHE-9808182 for computations) is gratefully acknowledged. Thanks are due to Professor Aron Kuppermann and Dr. Phil Mayer for a helpful discussion of tunneling effects and an anonymous reviewer for a discussion of hot atom kinetics.

**Supporting Information Available:** Figures S1−S22 with potential energy profiles, Eckart functions, and Arrhenius plots for model 4 reactions, Tables S1−S69 with optimized geometries in Cartesian coordinates (PDF). This material is available free of charge via the Internet at http://pubs.acs.org.

JA021162T